Energy Conversion and Management 335 (2025) 119837

Contents lists available at ScienceDirect

Energy Conversion and Management

journal homepage: www.elsevier.com/locate/enconman

Research Paper

A comparative overview of various single-shaft and parallel-flow Brayton cycles developed from turbochargers

C.C. Cockcroft, W.G. Le Roux *

Department of Mechanical and Aeronautical Engineering, University of Pretoria, Private Bag X20, Hatfield, Pretoria 0028, South Africa

ARTICLE INFO

Keywords:
Brayton cycle
Turbocharger
Concentrating solar power
Recuperation
Single-shaft
Parallel-flow

ABSTRACT

Automotive turbochargers can be used to develop gas turbine cycles; however, turbochargers operate at low pressure ratios where cycle performance is sensitive to the addition of pressure-drop components. Parallel-flow Brayton cycles have been proposed to reduce the effect of pressure losses on cycle performance. This analytical study therefore compares various parallel-flow Brayton cycle configurations to their single-shaft counterparts, considering combustion, recuperation, as well as a concentrated solar power input via a solar dish and an open-cavity tubular receiver to identify where parallel-flow cycles are advantageous. Results show that the main shaft turbocharger choice greatly influences whether a single-shaft or a parallel-flow cycle is more beneficial. In recuperated solar cycles with a 6 % combustion chamber pressure loss, the parallel-flow low-temperature-turbine configuration with the solar receiver before the power turbine (in parallel with the main shaft) can achieve a peak thermal efficiency of 23.5 %, with 3 kW of power output, at a pressure ratio of 1.6. This can be compared with a peak thermal efficiency of 21.8 % at a pressure ratio of 1.75 for its single-shaft counterpart. In recuperated parallel-flow cycles and recuperated solar parallel-flow cycles, thermal efficiency performance improves under increased combustion chamber pressure losses, from 6 % up to 11 %, in contrast to the declining performance of single-shaft cycles. More specifically, at a pressure ratio of 1.8, results show that the parallel-flow low-temperature-turbine configuration can outperform its single-shaft counterpart when combustion chamber pressure losses exceed 8.7 %. The study highlights the potential of parallel-flow Brayton cycles for recuperation and concentrated solar power integration, particularly in low-pressure-ratio systems, offering practical guidance for turbocharger and cycle configuration selection.

1. Introduction

Global environmental sustainability is threatened by pollution caused by high energy consumption [1]. The efficient use of renewable energy sources, such as solar energy, forms a viable power generation alternative to traditional power generation methods, while reducing the reliance on fossil fuel energy production [2]. The utilisation of solar energy is a valuable consideration as solar energy is available as a low-cost and abundant source of energy with wide global availability [3]. Many commercial power generation systems are constructed based on open-air Brayton cycles, also known as gas turbine cycles [4]. These gas turbine cycles are advantageous in terms of being lightweight and compact for small-scale implementation [5].

Gas turbine cycles can be constructed with added cogeneration and solar hybridisation components, to both improve the system and meet global sustainability goals [6], but this comes at the expense of greater pressure losses [7]. In further extension of improving the sustainability of a gas turbine cycle, some of the required combustion heat in a gas turbine cycle can be supplemented through recuperating the high temperature exhaust gas from the cycle [8]. This allows for greater cycle thermal efficiency and lower gas emissions due to a lower utilisation of fuel in the combustion process [9]. However, this process is achieved through the use of an added pressure loss component in the form of a recuperator, which subsequently results in more cycle pressure losses [10].

Commercial automotive turbochargers can be used as the compressor and turbine in gas turbine cycles, as was done in the development of the commercial 3 kW combined heat and power plant by Visser et al. [11]. This has also been considered in the studies by Le Roux [12], Le Roux & Sciacovelli [13], Butt et al. [14], De Beer et al. [15], and Van Der Merwe et al. [16]. Radial automotive turbochargers can be beneficial to represent the microturbine in a gas turbine cycle due to the radial flow structure of radial turbomachinery allowing for enough

* Corresponding author.
E-mail address: willem.leroux@up.ac.za (W.G. Le Roux).

https://doi.org/10.1016/j.enconman.2025.119837
Received 19 December 2024; Received in revised form 25 March 2025; Accepted 21 April 2025
Available online 6 May 2025

Nomenclature

Symbols

A	Area [m^2]
a	Recuperator channel width [m]
b	Recuperator channel height [m]
d	Tube diameter [m]
F	View factor
f	Friction factor
H	Height [m]
h	Specific enthalpy [J/kg]
K	Loss coefficient
k	Thermal conductivity [W/mK]
L	Length [m]
$\dot{m}$	Mass flow rate [kg/s]
N	Number of tube sections
P	Pressure [Pa]
$\dot{Q}$	Heat transfer rate [W]
T	Temperature [K]
t	Thickness [m]
$\dot{W}$	Rate of work [W]

Greek symbols

ε	Emissivity
η	Efficiency
λ	Heat transfer coefficient [W/m^2K]
σ	Stefan-Boltzmann constant [W/m^2K]

Subscripts

0	Ambient
1–9	States 1–9
CC	Combustion chamber
comp	Compressor
cond	Conduction
conv	Convection
gt	Gas turbine
in	Inlet
ins	Insulation
loss	Loss
LPG	Liquified Petroleum Gas
n	Tube section number
net	Net amount
o	Outer
out	Outlet
pt	Power turbine
rad	Radiation
rec	Recuperator
recv	Receiver
s	Surface
th	Thermal
y	Elbow number

Superscripts

*	Solar

Abbreviations

(SR-CC)	Solar receiver placement 1 (before the *CC*)
(SR-PT)	Solar receiver placement 2 (before the *PT*)
AR	Aspect Ratio
CC	Combustion Chamber
CSP	Concentrating Solar Power
EUF	Energy Utilisation Factor
G	Generator
GT	Gasifier Turbine
HTT	High-Temperature Turbine
ITT	Intermediate-Temperature Turbine
ITT(S)	Intermediate-Temperature Turbine (Solarised)
LPG	Liquefied Petroleum Gas
LTT	Low-Temperature Turbine
NTU	Number of Transfer Units
PT	Power Turbine
SR	Solar Receiver
SS	Single-Shaft
TIAC	Turbine Inlet Air Cooling

space for the addition of other components [7] for recuperation, solar hybridisation, and further cogeneration use [17]. However, the use of these off-the-shelf turbochargers only allows for operation at low pressure ratios. At low pressure ratios pressure losses have a greater influence on the cycle results in single-shaft configurations due to enforcing a greater proportional reduction in the pressure ratio through the cycle turbine [16]. Additionally, these low pressure ratios are too low for the operation of a twin-shaft cycle due to the pressure ratios through both the gasifier and power turbine being too low for feasibility when automotive turbochargers are used [16]. For example, the initial novel experimental single-shaft solar-dish gas turbine cycle study by Swanepoel et al. [18] showed feasibility for a solar-dish Brayton cycle, but the added components for the application of recuperation, thermal energy storage, and additional piping in the cycle did not offer feasible power generation results in comparison to a simple solar gas turbine cycle configuration. However, concentrating solar power (CSP) and recuperation should form viable cycle additions when it comes to improving thermal efficiency and reducing the environmental impact of cycle operation [19].

Parallel-flow cycles [16] form a solution to the detrimental performance results that pressure losses add to a single-shaft or a twin-shaft gas turbine cycle [20]. This is done through a minimised pressure loss effect on the pressure ratio through the power turbine, while maintaining the operational flexibility and independent turbine shaft speeds of a twin-shaft cycle [21]. This minimised pressure loss effect is as a result of separating the cycle flow rates into two individual streams so that the cycle components, consisting of the combustion chamber, recuperator, and solar receiver, in the current study, can be placed along different flow streams. These two individual flow stream options allow for the pressure losses caused by pressure loss components to be better distributed. This ascertains that the pressure ratios through one or both of the turbines can be maximised.

Various simple and recuperated parallel-flow Brayton cycles developed from turbochargers have been introduced and investigated by Van der Merwe et al. [16]. This concept has further been expanded into an analysis of turbine inlet air cooling by Cockcroft & Le Roux [22], into an analysis of recuperation on parallel-flow cycle setups by Cockcroft & Le Roux [23], and into an analysis on the effect of solar receiver placement in simple and recuperated parallel-flow Brayton cycle configurations by Cockcroft & Le Roux [19]. These studies introduced various parallel-flow cycles with the configuration being dependent on the placement of the parallel-flow split-off point and the placement of the solar receiver in the various solar cycles. The split-off point and solar receiver placements have been shown to greatly influence the results that are obtained in the operation of the cycles. These configurations consisted of the low-temperature turbine (LTT), intermediate-temperature turbine (ITT), intermediate-temperature turbine (solarised) (ITT(S)), and high-temperature turbine (HTT) configurations – depending on the placement of the cycle split-off point. Additionally, the solar receiver was placed either before the combustion chamber or before the power

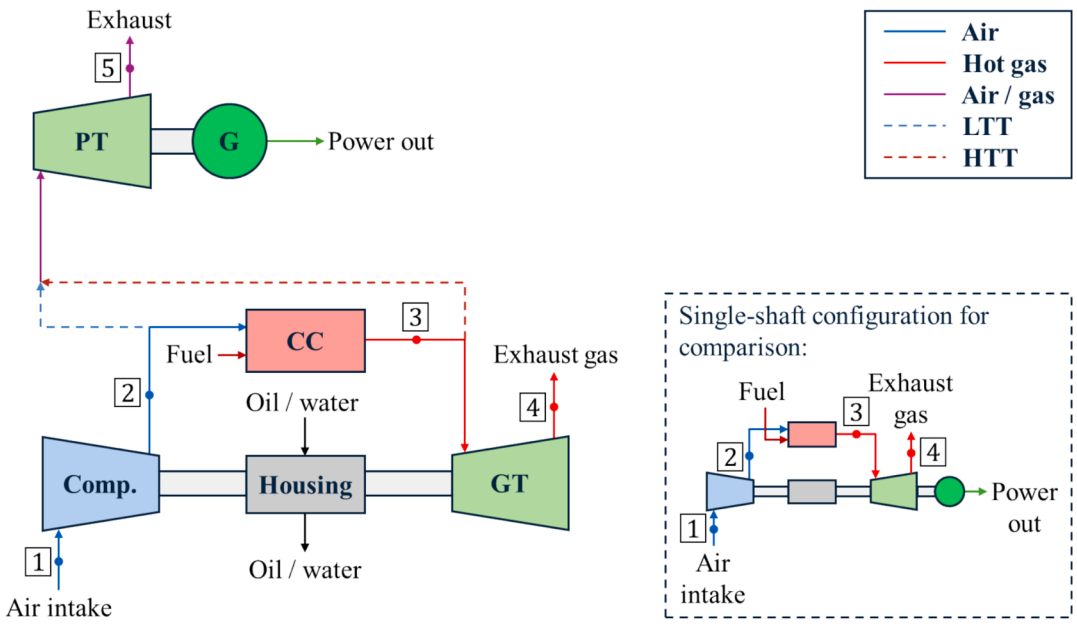

Fig. 1. Simple cycle parallel-flow and single-shaft configurations, adapted from Ref. [22].

turbine.

1.1. Novelty and contribution

Although the configurations introduced by Cockcroft & Le Roux [19,23] have been extensively investigated, these cycles have not been compared to their various single-shaft counterparts. Thus, the current study forms its novelty through comparing the various parallel-flow and single-shaft cycle configurations developed from turbochargers through analysing the responses of the various cycle configurations to added cycle pressure losses. To the authors' knowledge, a comparison of this nature, through comparing various single-shaft and parallel-flow cycles to one another on a per pressure ratio and on a pressure loss percentage basis, has not been done before. These comparisons are necessary to determine the best-case cycle configuration, in a single-shaft or parallel-flow setup, to maximise thermal efficiency. A higher efficiency indicates that more power output is obtained from the fuel input. Thus, this is an important consideration to be made regarding whether a parallel-flow cycle is capable of outperforming a single-shaft cycle, when considering different cycle types.

2. Methodology

For an analytical investigation regarding the various parallel-flow and single-shaft Brayton cycle configurations, the cycle layouts and cycle components for analysing the air-operated gas turbine cycles are presented. Each cycle is solved through its own Python algorithm through the consideration of different pressure ratios. For the simple, recuperated, and recuperated solar cycles, the pressure ratios are simulated based on a Python array, *[1.4, 1.5, 1.6, 1.8, 2.0, 2.25, 2.5]*, as done in the study by Cockcroft & Le Roux [19].

When a recuperator is considered in a cycle setup, a flat-plate recuperator is used (as defined in the recuperator analysis below). This flat-plate recuperator makes use of n channels in a single-direction, with n being subjected to a Python array of *[15, 22.5, 30, 37.5, 45]*. The channel height options for the flat-plate recuperator are inputted into Python as an array (*[1.50, 2.25, 3.00, 3.75, 4.50]*) of channel height options in millimetres. The remaining recuperator geometry is detailed in the recuperator section to follow.

Considering the above input arrays and the component analysis requirements to be introduced in section 2.2, each cycle configuration in this study is solved for iteratively with the solution being obtained when the required tolerance is satisfied. This procedure stems from the manner in which Van der Merwe et al. [16] have solved for similar cycles, with a verification procedure having been done in the study by Cockcroft & Le Roux [22].

2.1. Cycle layouts

Different simple, recuperated, simple solar, and recuperated solar parallel-flow and single-shaft configurations are considered in this study. The simple and recuperated parallel-flow cycles have already been analysed by Van der Merwe et al. [16] and Cockcroft & Le Roux [23], while the simple solar and recuperated solar cycles have already been analysed by Cockcroft & Le Roux [19]. Thus, these cycles are not fully detailed and investigated in the current study, but their various configurations are still included and detailed for reference and comparison to their single-shaft counterparts.

Prior to a discussion of the various cycle types, the naming conventions used in the parallel-flow cycles need to be detailed. The names associated with the parallel-flow cycles are determined from the location of their parallel-flow split-off point, as detailed in the studies by Cockcroft & Le Roux [19,23]. A low-temperature turbine (LTT) configuration is formed when the split-off point occurs directly after the compressor. An intermediate-temperature turbine (ITT) cycle has a parallel-flow split-off point directly after the recuperator cold-side outlet. An intermediate-temperature turbine (solarised) cycle – ITT(S) cycle – has a parallel-flow split-off point directly after the solar receiver outlet. A high-temperature turbine (HTT) configuration is formed when the split-off point occurs directly after the combustion chamber. Various solar receiver placements are investigated for the parallel-flow solar cycles, as in the study by Cockcroft & Le Roux [19], with the first receiver placement occurring in the main cycle section and being indicated as (SR-CC) in the cycle naming convention. The alternative receiver placement occurs between the split-off point and the power turbine and is indicated as (SR-PT) in the cycle naming convention. These plant scheme configurations are further detailed in the subsections to follow. Note that in the plant scheme figures in the subsections to follow, a dashed line indicates that the flow is unique to the indicated cycle type, while solid lines indicate that the flow lines are active in each configuration of the cycle type.

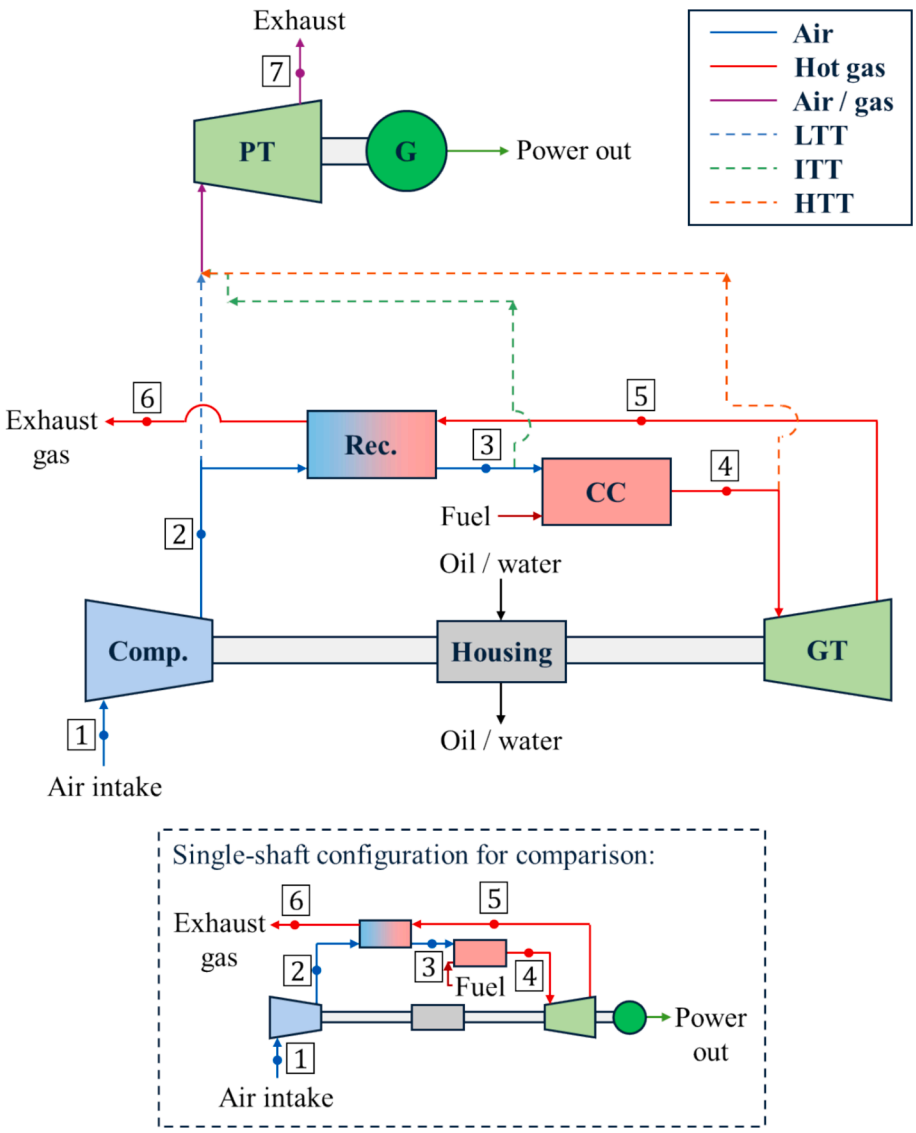

Fig. 2. Recuperated cycle parallel-flow and single-shaft configurations, adapted from Ref. [23].

2.1.1. Simple layouts

The first cycle type to be discussed is the simple cycle. In the simple cycle, there are two possible parallel-flow cycles, an LTT cycle and an HTT cycle, as detailed by Van der Merwe et al. [16]. Both of these cycles make use of a power turbine that is completely excluded from the single-shaft configuration, as indicated via Fig. 1. In the single-shaft configuration, the power output is obtained from the gasifier turbine, but the gasifier turbine also powers the coupled compressor, so the power output is obtained from the difference between the power generated in the gasifier turbine and the power required to operate the compressor. In contrast to this, the parallel-flow gasifier turbine is fully responsible for powering the compressor with the power output only being obtained from the power generated in the power turbine.

2.1.2. Recuperated cycle layouts

When a recuperated cycle configuration is used, there are three possible parallel-flow configurations, as detailed in the study by Cockcroft & Le Roux [23]. These parallel-flow configurations consist of a recuperated LTT cycle, an ITT cycle, and a recuperated HTT cycle, as shown in Fig. 2. This figure illustrates the possible cycle split-off points when a recuperator is incorporated into the setup and shows the single-shaft counterpart for reference. These configurations are explained in more detail in the study by Cockcroft & Le Roux [23]. As in the simple single-shaft layout, the recuperated single-shaft layout does not have a power turbine for operation, but the remaining main cycle section is the same as in the parallel-flow recuperated cycles, except the gasifier turbine is responsible for powering the compressor and producing the net power output in the single-shaft configuration.

2.1.3. Simple solar cycle layouts

The simple solar parallel-flow cycles utilise a solar receiver and have alternative solar receiver placements as analysed in the study by Cockcroft & Le Roux [19]. These alternative receiver placements are visualised as in Fig. 3 and Fig. 4, with Fig. 3 showing that when the receiver is placed prior to the combustion chamber inlet, there are three possible parallel-flow configurations, and one single-shaft configuration. This figure illustrates the possible cycle split-off points when a solar receiver is incorporated into the setup prior to the combustion chamber inlet and shows the single-shaft counterpart for reference. The parallel-flow cycles that make use of the first receiver placement are the LTT (SR-CC), the ITT(S) (SR-CC), and the HTT (SR-CC) cycles. For the alternative receiver placement in Fig. 4, there are two possible parallel-flow cycles, the LTT (SR-PT) cycle and the HTT (SR-PT) cycle. This figure illustrates the possible cycle split-off points when a solar receiver is incorporated

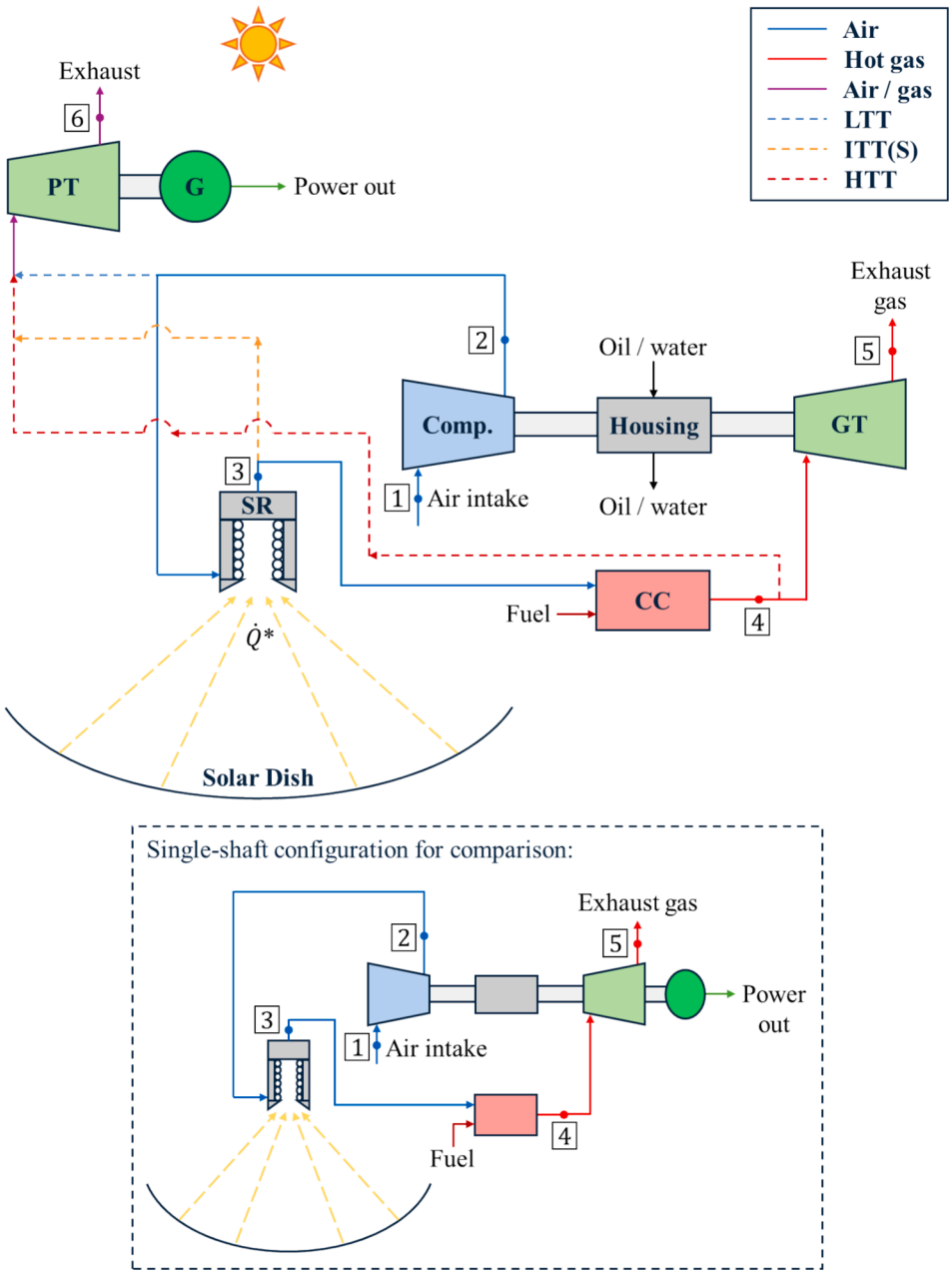

Fig. 3. Simple solar cycle parallel-flow and single-shaft configurations (SR-CC), adapted from Ref. [19].

into the setup prior to the power inlet and shows the single-shaft counterpart for reference. The same concepts as in the simple and the recuperated cycle layouts apply to the single-shaft layout in Fig. 3, with the power output being based on the difference between the gasifier turbine generated power and the power required to operate the compressor. The various simple solar cycle configurations are explained in more detail in the study by Cockcroft & Le Roux [19].

2.1.4. *Recuperated solar cycle layouts*

For the recuperated solar cycle layouts, there are two possible solar receiver placements in the various parallel-flow configurations as detailed in the study by Cockcroft & Le Roux [19]. These alternative placements are shown in Fig. 5 and in Fig. 6. Fig. 5 shows that when the first receiver placement is used, with the solar receiver being placed between the cold-side outlet of the recuperator and the combustion chamber inlet, there are four possible parallel-flow layouts that can be compared to the single-shaft configuration. These parallel-flow layouts consist of the recuperated solar LTT (SR-CC), the recuperated solar ITT (SR-CC), the recuperated solar ITT(S) (SR-CC), and the recuperated solar HTT (SR-CC) configurations. For the second receiver placement, with the solar receiver placed between the cycle split-off point and the power turbine inlet, there are three possible parallel-flow configurations, the recuperated solar LTT (SR-PT), the recuperated solar ITT (SR-PT), and the recuperated solar HTT (SR-PT) configurations. The single-shaft power output is again determined as the difference between the power generated in the gasifier turbine and the power required to operate the compressor.

2.2. *Component analysis*

The components that make up the various cycle configurations in the current study are defined in the same manner as in the studies by Cockcroft & Le Roux [19,22,23], with a consideration of pressure losses on a per component basis. The cycles utilise an intake of air at state 1,

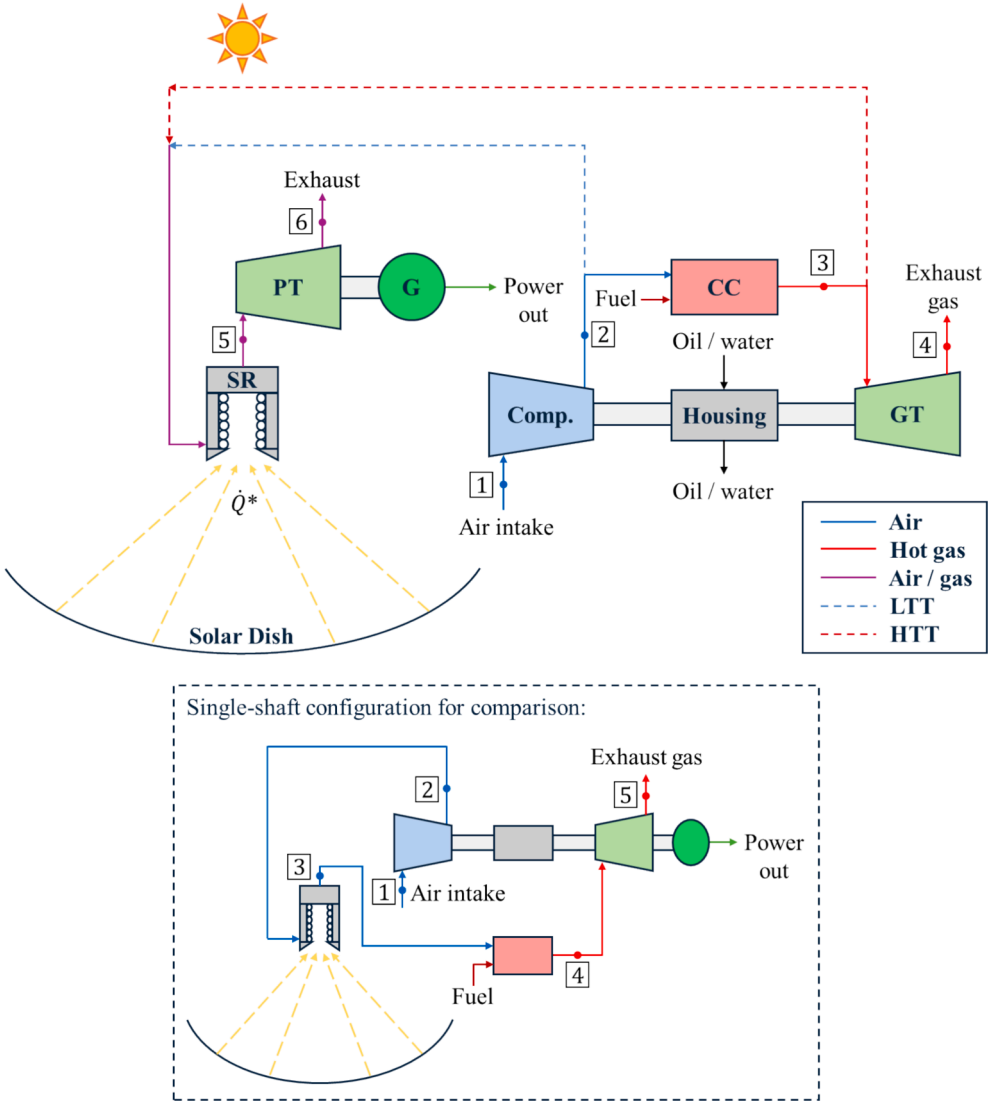

Fig. 4. Simple solar cycle parallel-flow configurations (SR-PT), adapted from Ref. [19].

with this air being the same as the ambient air in Pretoria, South Africa, and having a subsequent ambient pressure of 86.6 kPa and an ambient temperature of 300 K [24]. The cycles all exhaust to the ambient pressure. In this study, note that the alternative application of the turbochargers results in various operating points within the turbomachinery flow maps. This means that the results from the turbomachinery flow maps are obtained via determining the off-design operating points of the turbocharger components. Thus, the impact of off-design conditions is considered regarding their influence on machine efficiency, as done in the study by Cockcroft & Le Roux [22].

The power output of the parallel-flow cycles is determined as per Equation (1), with the single-shaft cycle power outputs being determined as per Equation (2). For both the parallel-flow and the single-shaft cycles, the thermal efficiency is determined as per Equation (3), through considering the heat transfer that occurs in the combustion chamber. Note that for the solar cycles, the thermal efficiency would typically include the solar heat added to the cycles in the denominator of Equation (3). However, this would not give a clear indication of the power output obtained with reference to the fuel added to the cycle. Thus, for the solar cycles, the thermal efficiency determined via Equation (3) is actually the fuel-based thermal efficiency as detailed in the study by Cockcroft & Le Roux [19]. For the purpose of the current study, all thermal efficiencies are determined using Equation (3) for simplicity.

$$\dot{W}_{net} = \dot{W}_{gt} + \dot{W}_{pt} - \dot{W}_{comp} = \dot{W}_{pt} \tag{1}$$

$$\dot{W}_{net} = \dot{W}_{gt} - \dot{W}_{comp} \tag{2}$$

$$\eta_{th} = \frac{\dot{W}_{net}}{\dot{Q}_{CC}} \tag{3}$$

2.2.1. Compressor and turbines

Commercially available automotive turbochargers are used to represent the compressor and gasifier turbine as a coupled pair in the parallel-flow and single-shaft layouts. This characterisation is thus done using the compressor and exhaust flow maps of the commercially available turbomachinery to extract values for further mathematical use when it comes to determining the isentropic efficiencies and mass flow rates of the compressor and turbines in this study. Thus, the performance of the compressors and turbines in the various cycles is directly determined by their turbomachinery flow maps and differs for each design point.

Due to the existence of the additional power turbine in the parallel-flow configurations, a separate turbocharger is used to model the power turbine [16]. To represent these turbomachinery components, two different *Garret Motion* [25] turbochargers are used for the coupled main

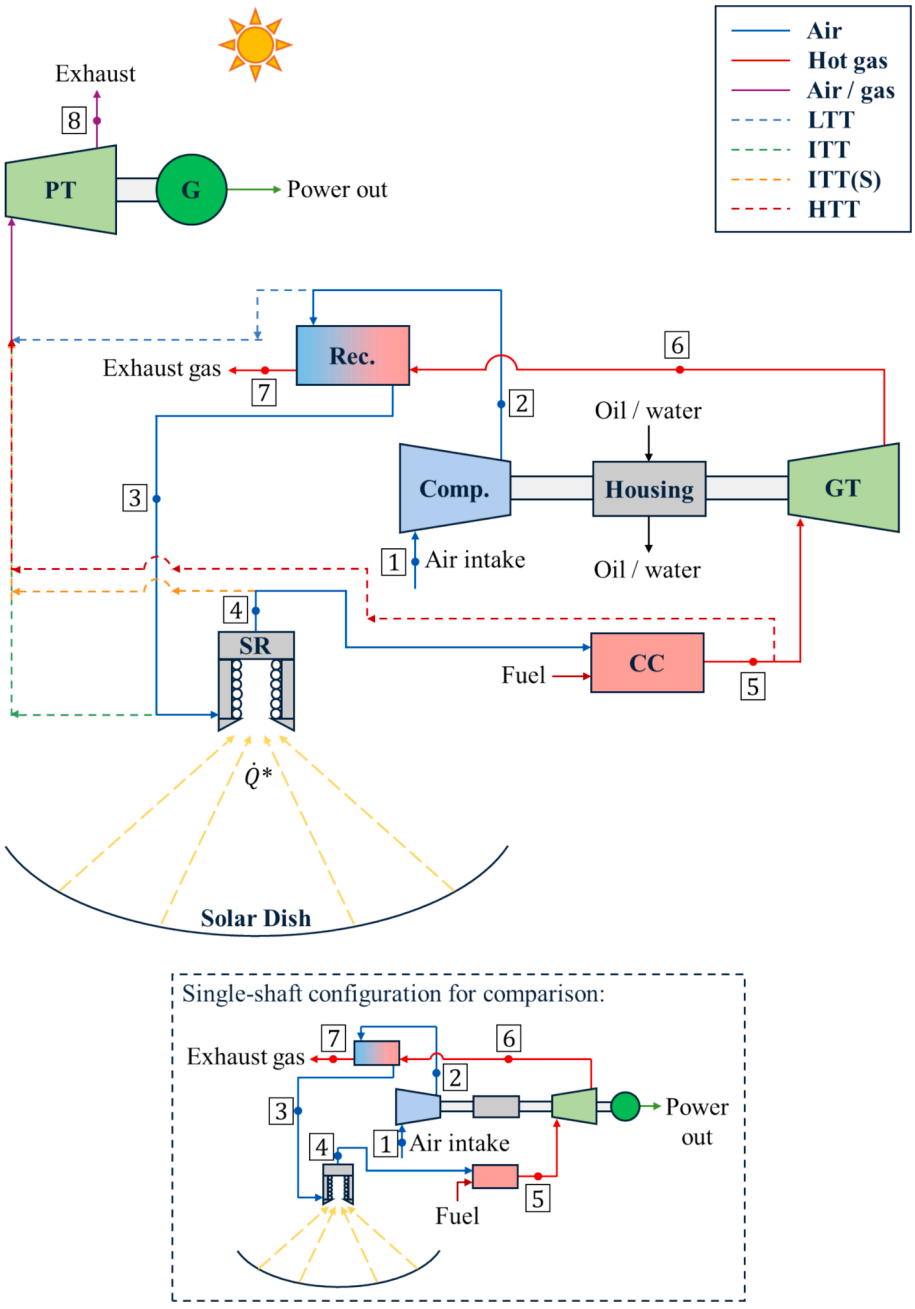

Fig. 5. Recuperated solar cycle parallel-flow and single-shaft configurations (SR-CC), adapted from Ref. [19].

shaft compressor and gasifier turbine, namely the G25-550 (AR = 0.92) and the GTX4088R (AR = 1.19) turbochargers. The power turbine in the parallel-flow configurations are simulated based on the *Garret Motion* [25] GBC14-200 and GBC17-250 turbochargers as power turbine options for both main shaft turbochargers. These turbochargers and turbocharger combinations are selected based on numerous simulations with other turbochargers and combinations, with the mentioned turbochargers offering the best compatibility results for a wide range of configurations and cycle types. Moreover, the exact simulation and calculation procedures for the turbomachinery in this study follows the in-depth contour mapping and *Webplotdigitizer* [26] digitisation procedures as detailed in the studies by Cockcroft & Le Roux [19,22,23].

Lastly, when using Garrett Motion turbochargers, the turbine inlet temperature may not exceed 950 °C due to manufacturer limitations [27]. The current study considers this temperature as 1200 K (927 °C) for a conservative simplification and this limit is used to model the inlet temperatures to the single-shaft gasifier turbine in the various single-shaft cycles, as done by Le Roux & Meyer [28]. This is considered for the gasifier turbine inlet temperatures associated with each cycle configuration type and is also considered for the power turbine inlet.

2.2.2. *Combustion chamber*

To model the combustion chamber in the current study, the chemical reaction equation for the combustion between injected liquified petroleum gas (LPG) and air is used. The standard formulation of 60 % propane and 40 % butane is used to represent the LPG formulation, as per standard LPG formulation in South Africa [29]. The molar relations between the reactants and the products in the chemical reaction equation are solved for via interpolation and a consideration of the mass added to the cycle in the combustion process and the adiabatic flame temperature required to balance the gasifier turbine and compressor work rates, for the various parallel-flow cycles, as detailed in-depth in

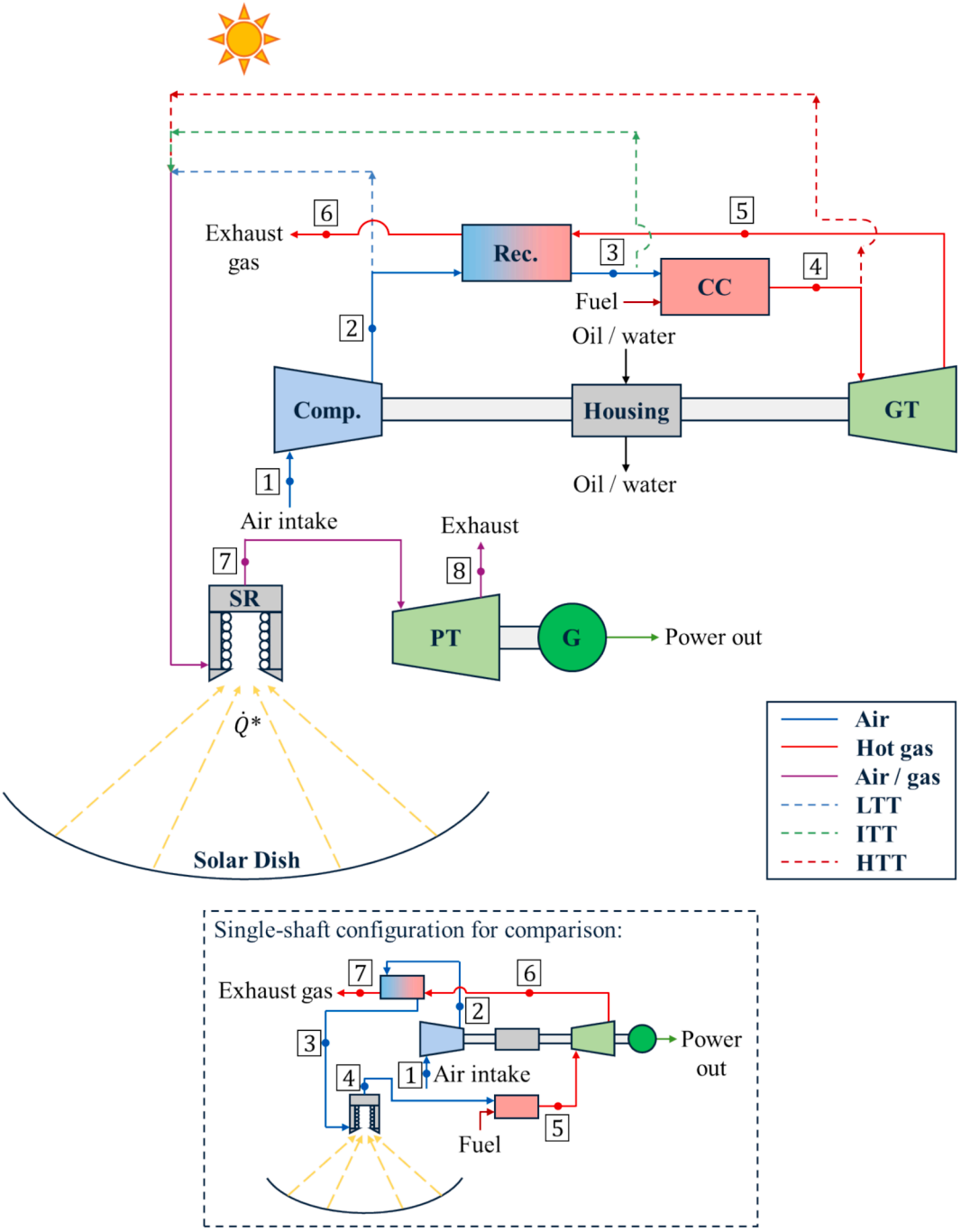

Fig. 6. Recuperated solar cycle parallel-flow configurations (SR-PT), adapted from Ref. [19].

the study by Cockcroft & Le Roux [22]. For the single-shaft cycles, the gasifier turbine inlet temperature is restricted to 1200 K and thus is not solved for iteratively as in the parallel-flow cycles, but the solution setup for the single-shaft combustion solution procedure remains the same as in the parallel-flow analysis. Note that a control system would be required to either maintain the gasifier turbine inlet temperature at 1200 K in a single-shaft cycle or to ascertain that the gasifier turbine inlet temperature is equal to the required value to allow for the gasifier and compressor power amounts to equate to one another in the instance of a parallel-flow cycle. This is required to optimise the system performance.

Lastly, according to Lefebvre & Ballal [30], the pressure loss in an annular combustion chamber equates to approximately 6 % of the pressure entering the combustion chamber. However, in the experimental analysis by Swanepoel et al. [18], this pressure loss was found to be as high as 10.2 % when considering the combustion chamber (in a recuperated cycle) and the piping connections between the various components and the combustion chamber. Thus, the current study considers combustion pressure losses of between 6 % and 11 % for the various cycles consisting of the G25-550 (AR = 0.92) as the main shaft turbocharger to ascertain the performance of each parallel-flow and single-shaft cycle under greater amounts of combustion chamber pressure loss.

2.2.3. *Recuperator*

When a recuperator is used in a cycle configuration, the recuperator is defined as per the flat-plate recuperator model detailed by Le Roux & Sciacovelli [13], and per the model defined by Nellis & Pfotenhauer [31]

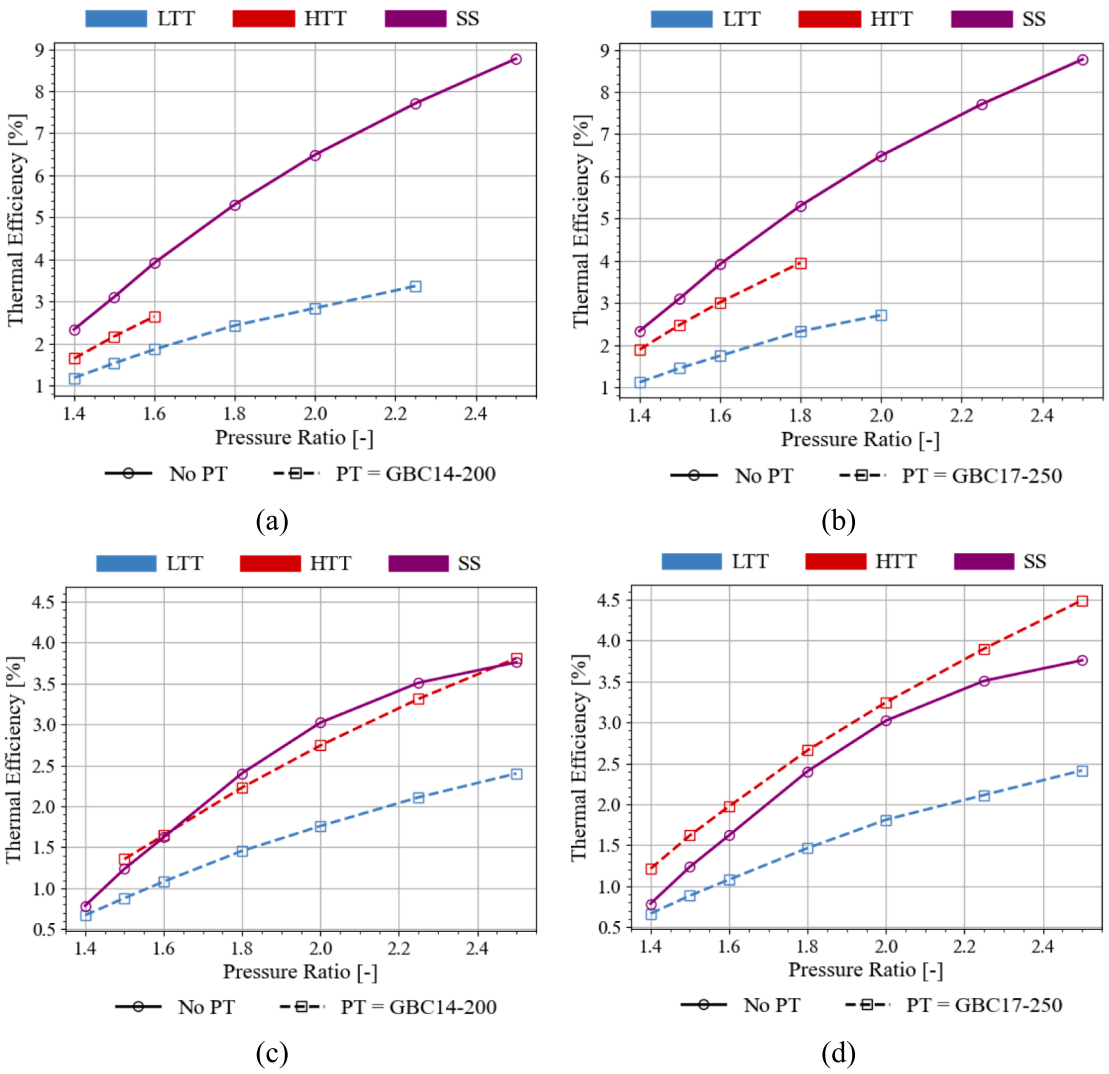

Fig. 7. Thermal efficiency as a function of pressure ratio in a simple cycle for (a) the G25-550 (AR = 0.92) as the GT and GBC14-200 as the PT, (b) the G25-550 (AR = 0.92) as the GT and GBC17-250 as the PT, (c) the GTX4088R (AR = 1.19) as the GT and GBC14-200 as the PT, and (d) the GTX4088R (AR = 1.19) as the GT and GBC17-250 as the PT.

– using the effectiveness-NTU heat exchanger solving method that includes heat loss to the environment. For reference regarding the recuperator dimensions, a is the recuperator width, b is the recuperator channel height, n is the number of channels in a single-direction, and L_{rec} is the length of the recuperator, as in the studies by Cockcroft & Le Roux [19,23]. The recuperator has a plate thickness, t, of 0.5 mm, and the length and width of the recuperator are kept constant at 1.5 m and 0.225 m, respectively. This has been detailed in Ref. [23]. Note that the input recuperator dimensions influence the pressure loss through the recuperation process. This pressure loss is determined as in the study by Le Roux & Sciacovelli [13].

2.2.4. Solar receiver

An open-cavity tubular solar receiver is used as detailed in Ref. [19]. This receiver utilises solar heat that is reflected into the receiver via a solar dish with a diameter of 4.8 m (with a dish area of 18 m^2), a reflectivity of 85 % and an optical error of 10 mrad, while assuming a direct normal irradiance of 1000 W/m^2 [32]. The specified geometry of the solar receiver is used to determine the pressure loss through the receiver with a consideration of the mass flow rate through the receiver as per the study by Le Roux et al. [32]. The solar rays that are reflected from the dish are traced using SolTrace [33], based on techniques for solar flux mapping [32]. Due to the material design restrictions of the solar receiver, the surface temperature of the tubes is not allowed to be greater than 1200 K [18]. This is analysed in the results pertaining to the solar cases. Under the consideration of conduction, convection, and radiation heat losses and gains, the resulting equation for determining the heat transfer that the solar receiver adds to the cycle is as per Equation (4). This equation is solved for via Gaussian elimination in Python, as done in the study by Le Roux et al. [32]. Moreover, the efficiency of the solar receiver is determined as per Equation (5) [32].

$$\dot{Q}_{net,n} = \dot{Q}_n^* - A_n \sum_{j=1}^{N} F_{n-j}\left(\varepsilon_n \sigma T_{s,n}^4 - \varepsilon_j \sigma T_{s,j}^4\right) - A_n F_{n-0}\left(\varepsilon_n \sigma T_{s,n}^4 - \varepsilon_j \sigma T_0^4\right) - \lambda_{recv,n} A_n \left(T_{s,n} - T_0\right) - \frac{A_n \left(T_{s,n} - T_0\right)}{\frac{1}{\lambda_o} + \frac{t_{ins.}}{k_{ins}}} \tag{4}$$

$$\eta_{SR} = \frac{\dot{Q}_{net}}{\dot{Q}^*} \tag{5}$$

3. Results

The various parallel-flow and single-shaft cycle results are presented and analysed in this section. The results of each cycle type consist of an

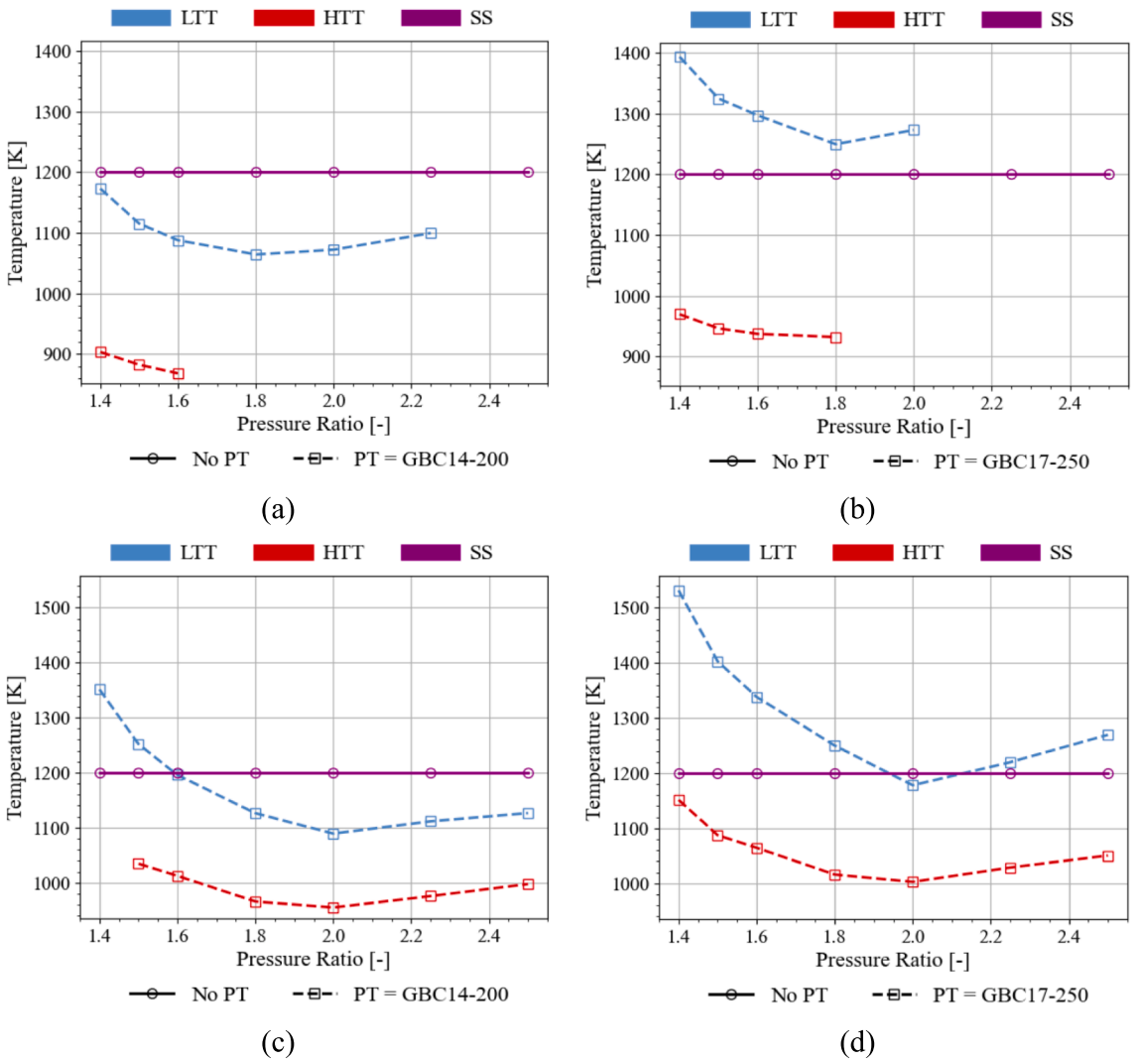

Fig. 8. GT inlet temperature as a function of pressure ratio in a simple cycle for (a) the G25-550 (AR = 0.92) as the GT and GBC14-200 as the PT, (b) the G25-550 (AR = 0.92) as the GT and GBC17-250 as the PT, (c) the GTX4088R (AR = 1.19) as the GT and GBC14-200 as the PT, and (d) the GTX4088R (AR = 1.19) as the GT and GBC17-250 as the PT.

analysis of the power outputs (shown in Appendix B for reference and discussions), thermal efficiencies, and temperature limitations. Thermal efficiency is of primary importance in this study and is greatly influenced by the cycle components. Thus, the recuperator effectiveness and solar receiver efficiency values are paramount when it comes to detailing the reasons as to why the thermal efficiency values deviate across the cycles. Appendices C and D can be referred to for the influence that these parameters have on the cycle results.

Two power turbine options with the G25-550 (AR = 0.92) and GTX4088R (AR = 1.19) main shaft turbocharger options are considered at different pressure ratios and at a combustion chamber pressure loss of 6 % for a cycle pressure ratio analysis. Note that for the main analysis, the thermal efficiency results of the various cycles are discussed to determine where the highest feasible thermal efficiency is obtained with reference to the various cycle temperatures that have been constrained to 1200 K.

For the G25-550 (AR = 0.92) main shaft turbocharger, additional investigations are done considering pressure losses from 6 % to 11 % for an analysis into the effect of increased combustion chamber pressure losses. The pressure loss analysis is based on the mid-range pressure ratio of 1.8 for the various cycles. This pressure ratio is considered for this analysis due to low gasifier turbine inlet temperatures, as observed by Cockcroft & Le Roux [19]. This is important because in the parallel-flow analyses by Van der Merwe et al. [16] and Cockcroft & Le Roux [22], it has been shown that an increase in pressure loss results in higher gasifier turbine inlet temperatures. Thus, it is better to operate at a pressure ratio with a lower turbine inlet temperature to remain within the limit of 1200 K.

Note that the various parallel-flow cycles have already been compared in the studies by Cockcroft & Le Roux [19,22,23] for the G25-550 (AR = 0.92) as the main shaft turbocharger. The relationships between the various parallel-flow cycles when the GTX4088R (AR = 1.19) is used as the main shaft turbocharger follow a similar relationship response to that of the G25-550 (AR = 0.92) main shaft turbocharger, unless different recuperator geometry (shown in Appendix A) is required to reduce the gasifier turbine inlet temperatures. Thus, this study primarily focusses on whether a parallel-flow cycle can outperform a single-shaft cycle, with a specific focus on thermal efficiency, and the conditions in which a parallel-flow cycle offers better results, with some minor modifications to the coding procedure by Cockcroft & Le Roux [19,22,23] for improved accuracy.

3.1. Simple cycle results

When the G25-550 (AR = 0.92) is used as the main shaft turbocharger, Fig. 7 shows that none of the parallel-flow cycles are able to

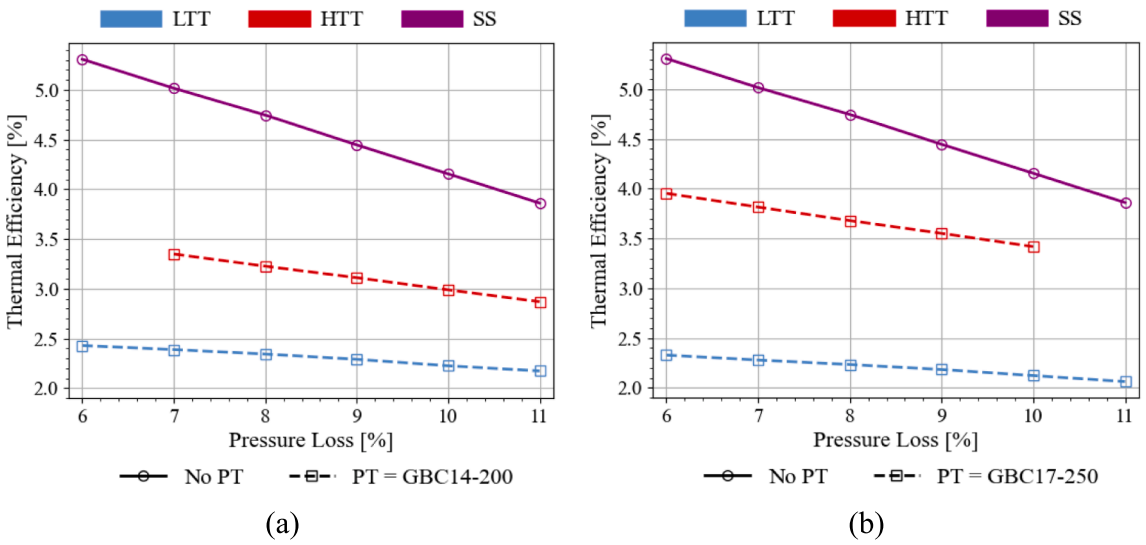

Fig. 9. Thermal efficiency as a function of pressure loss for the G25-550 (AR = 0.92) as the GT in a simple cycle at a compressor pressure ratio of 1.8 with (a) the GBC14-200 as the PT and (b) the GBC17-250 as the PT.

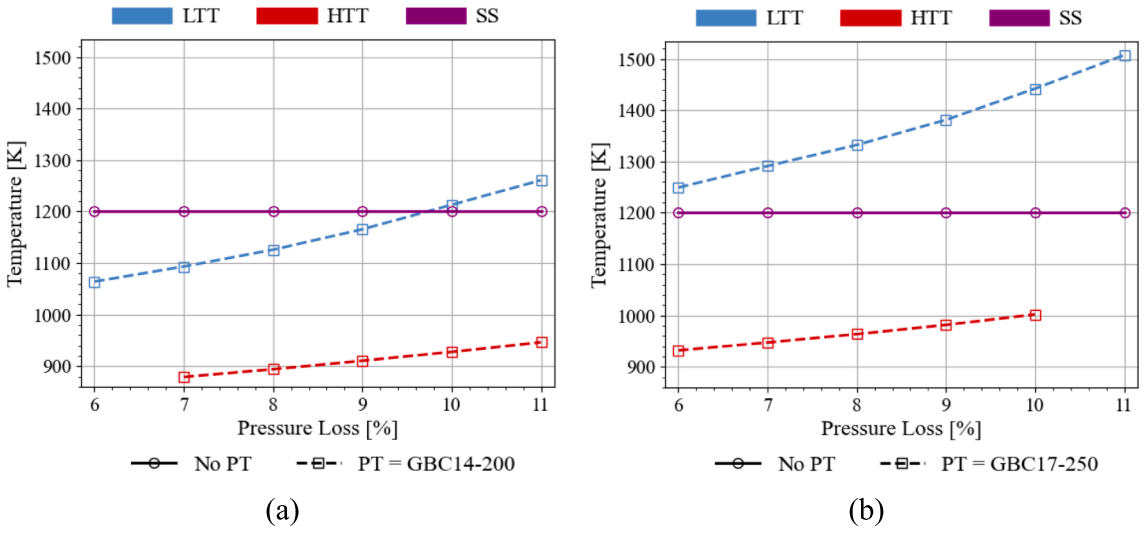

Fig. 10. GT inlet temperature as a function of pressure loss for the G25-550 (AR = 0.92) as the GT in a simple cycle at a compressor pressure ratio of 1.8 with (a) the GBC14-200 as the PT and (b) the GBC17-250 as the PT.

provide higher thermal efficiencies than the single-shaft cycle for either power turbine options. Additionally, the compressor pressure ratio range of the parallel-flow cycles is much shorter than in the operation of the single-shaft cycle, with the single-shaft cycle being able to produce much higher thermal efficiencies than the various parallel-flow cycles due to being able to operate up to a pressure ratio of 2.5. Moreover, the gasifier turbine inlet temperatures are too high at low pressure ratios for the LTT cycle with the GBC17-250 as the power turbine, as shown in Fig. 8(b).

Via Fig. 7, it is shown that, when the GTX4088R (AR = 1.19) is used as the main shaft turbocharger, the thermal efficiency results between the various configurations show that the GBC14-200 power turbine mostly does not provide better thermal efficiencies than the single-shaft cycle, except at pressure ratios of 1.5 – 1.6 and 2.5 when the HTT configuration is used. The HTT configuration with the GBC17-250 provides the highest thermal efficiencies out of all the plotted configurations for the entire pressure ratio range. This results in a maximum thermal efficiency of 4.49 % when using the HTT configuration with the GBC17-250 as the power turbine at a pressure ratio of 2.5. Fig. 8 also shows that this HTT cycle requires gasifier turbine inlet temperatures within the required limit of 1200 K for the entire pressure ratio range, and thus the HTT cycle is feasible for operating within the temperature limitations.

3.1.1. *Effect of pressure drop on the simple cycle results*

In terms of a pressure loss analysis, when the G25-550 (AR = 0.92) is used as the main shaft turbocharger, it is shown via Fig. 9 that even though the single-shaft cycle shows the greatest decline in thermal efficiency, none of the parallel-flow cycles are able to obtain higher thermal efficiencies than the single-shaft cycle at a pressure ratio of 1.8. Fig. 10(a) and Fig. 10(b) show that the HTT cycle has gasifier turbine inlet temperatures that are sufficiently within the required gasifier turbine inlet temperature at high pressure loss percentages. Thus, under even higher pressure losses, it is not expected that the temperature limit will be exceeded for the HTT cycle. This is not observed for the LTT cycle, as shown in Fig. 10(a) and Fig. 10(b), with the LTT cycle with the GBC14-200 power turbine exceeding the gasifier turbine inlet temperature limit at pressure losses above 9.6 %, and with the LTT cycle with

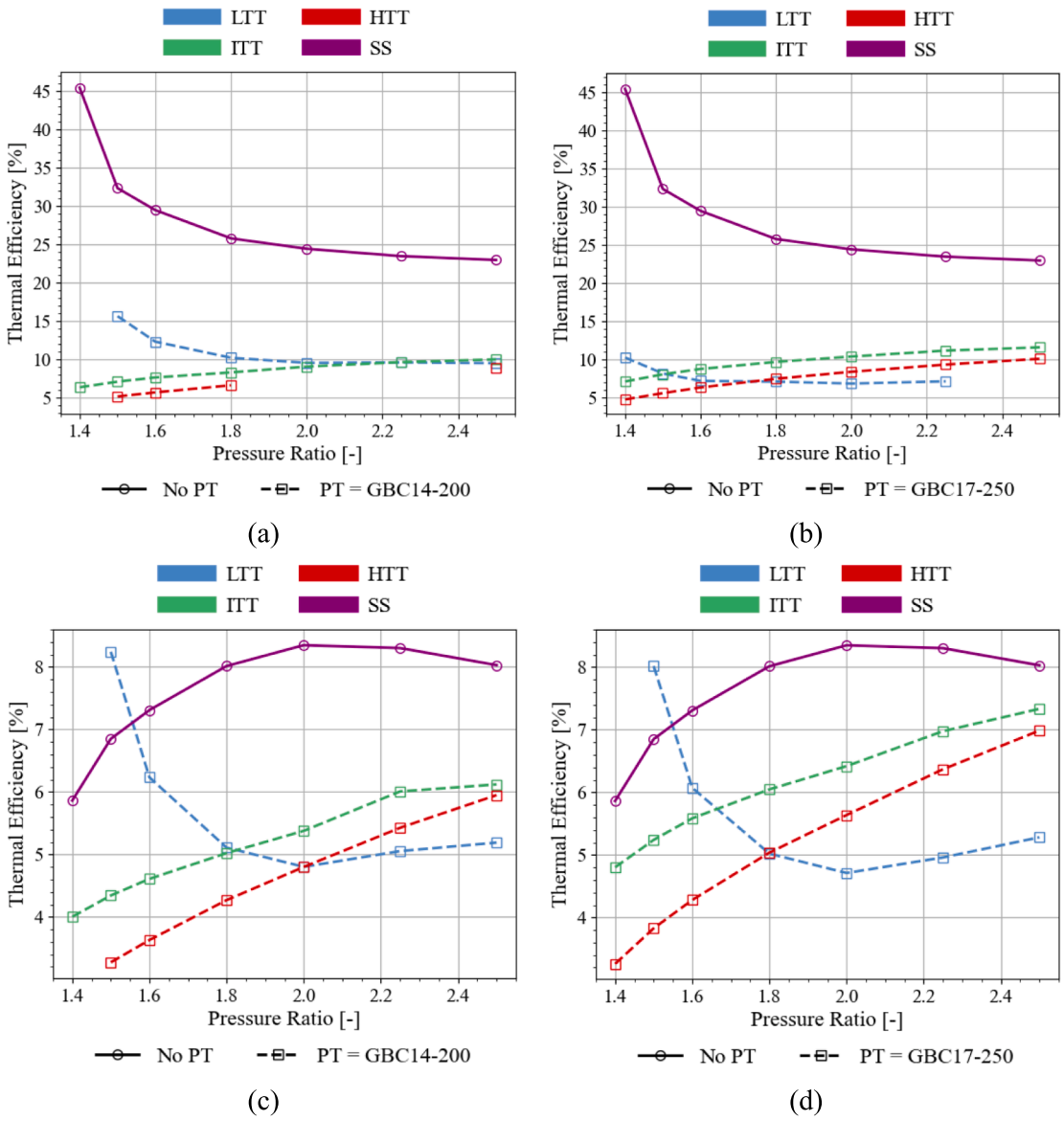

Fig. 11. Thermal efficiency as a function of pressure ratio in a recuperated cycle for (a) the G25-550 (AR = 0.92) as the GT and GBC14-200 as the PT, (b) the G25-550 (AR = 0.92) as the GT and GBC17-250 as the PT, (c) the GTX4088R (AR = 1.19) as the GT and GBC14-200 as the PT, and (d) the GTX4088R (AR = 1.19) as the GT and GBC17-250 as the PT.

the GBC17-250 power turbine exceeding the temperature limit for all considered pressure losses.

3.2. *Recuperated cycle results*

In terms of thermal efficiency, for the G25-550 (AR = 0.92) as the main shaft turbocharger, Fig. 11 shows that none of the parallel-flow cycles are able to provide higher thermal efficiencies than the single shaft cycle, which obtains its maximum thermal efficiency of 45.44 % at a pressure ratio of 1.4. This thermal efficiency decreases with an increase in pressure ratio with the lowest single-shaft thermal efficiency of 22.97 % at a pressure ratio of 2.5. Thus, the single-shaft cycle fully outperforms the parallel-flow cycles in a recuperated setup, with the highest parallel-flow thermal efficiency of 15.65 % occurring at a pressure ratio of 1.5 for the LTT cycle with the GBC14-200 power turbine.

For the GTX4088R (AR = 1.19) as the main shaft turbocharger, it is shown via Fig. 11 that the LTT cycles have the highest thermal efficiencies at pressure ratios of 1.5, with the GBC14-200 power turbine option having a thermal efficiency of 8.24 % and the GBC14-200 power turbine option having a thermal efficiency of 8.02 %. However, Fig. 12 shows that at the pressure ratios where the LTT cycles have the highest thermal efficiencies, the gasifier turbine inlet temperatures are too high. Thus, the LTT cycle, for both the GBC14-200 and the GBC17-250 power turbine options, is not feasible for obtaining high thermal efficiencies within the maximum allowable gasifier turbine inlet temperature. Thus, the highest feasible thermal efficiency, of 8.35 %, is obtained for the single-shaft cycle, at a pressure ratio of 2, as shown in Fig. 11.

Via Fig. 12, it is shown, for the G25-550 (AR = 0.92) main shaft turbocharger, that all the discussed parallel-flow cycles, with the exception of the LTT cycle with the GBC17-250 power turbine, require gasifier turbine inlet temperatures within the limit of 1200 K. Thus, this gasifier turbine inlet temperature consideration does not deem most of the discussed parallel-flow results, with the exception of the LTT cycle with the GBC17-250 power turbine, as infeasible for implementation.

3.2.1. *Effect of pressure drop on the recuperated cycle results*

When considering higher pressure losses in the cycle, the single-

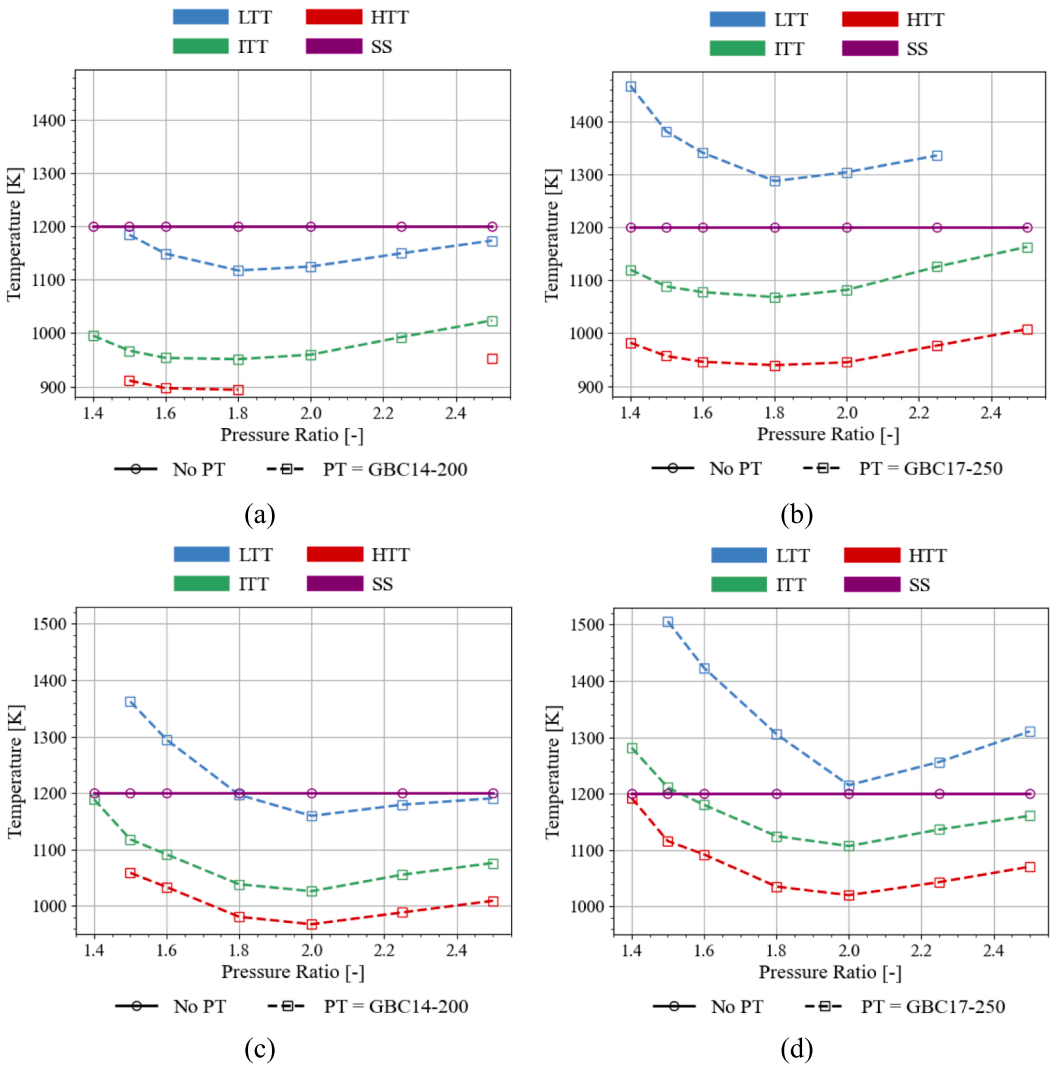

Fig. 12. GT inlet temperature as a function of pressure ratio in a recuperated cycle for (a) the G25-550 (AR = 0.92) as the GT and GBC14-200 as the PT, (b) the G25-550 (AR = 0.92) as the GT and GBC17-250 as the PT, (c) the GTX4088R (AR = 1.19) as the GT and GBC14-200 as the PT, (d) the GTX4088R (AR = 1.19) as the GT and GBC17-250 as the PT.

shaft, LTT, and HTT cycle thermal efficiencies respond in the same manner as in the simple cycle analysis, excluding the influence of recuperator dimensions (Appendix A), as shown in Fig. 13. The thermal efficiency of the ITT cycle increases with an increase in pressure loss. The gasifier turbine inlet temperatures of the parallel-flow cycles increase with an increase in pressure loss, which limits the LTT cycle, as shown in Fig. 14(a), with the gasifier turbine inlet temperature being too high for this cycle at pressure losses exceeding 9 %. Under these pressure loss considerations, the single-shaft cycle still performs the best with the thermal efficiency declining from 25.8 % at a pressure loss of 6 % to 21.8 % at a pressure loss of 11 % (with declining power outputs from 6.2 kW to 4 kW as per Fig. B4).

3.3. Simple solar cycle results

For the G25-550 (AR = 0.92) main shaft turbocharger in a simple solar cycle, Fig. 15 shows that none of the parallel-flow cycles offer better thermal efficiency than the single-shaft cycle. Thus, the best performance is obtained for in the single-shaft cycle, with a maximum power output of 20.7 kW (see Fig. B5) and a maximum thermal efficiency of 11.03 %, at a compressor pressure ratio of 3. At a compressor pressure ratio of 2.5, as the maximum simulated compressor pressure ratio for the other cycles, the simple solar single-shaft cycle generates 14.75 kW (see Fig. B5) of power with a thermal efficiency of 9.34 %. Note that the missing data observed in Fig. 15, particularly for the HTT (SR-CC) cycle, is as a result of incompatibility between the *Garrett Motion* turbocharger pairs. These incompatibilities are due to operational requirements beyond the bounds of either the main compressor map or the power turbine compressor map, as detailed by Van der Merwe et al. [16].

All the cycle configurations, with the G25-550 (AR = 0.92) as the main shaft turbocharger, with the exception of the LTT (SR-CC) cycle with the GBC14-250 as the power turbine at pressure ratios of less than 1.45, have gasifier turbine inlet temperatures, power turbine inlet temperatures, and solar receiver surface temperatures within the limit of 1200 K for the entire pressure ratio range. The LTT (SR-CC) and ITT(S) (SR-CC) cycles with the GBC17-250 as the power turbine, experience high gasifier turbine inlet temperatures throughout the operational pressure ratio range, as shown in Fig. 16.

When the GTX4088R (AR = 1.19) is used as the main shaft turbocharger, Fig. 15 shows that the LTT (SR-PT) cycle has the best thermal efficiency at low pressure ratios. However, when this cycle operates at low pressure ratios with the GBC17-250 power turbine, Fig. 16 shows that the gasifier turbine inlet temperature limit of 1200 K is exceeded. This is only an issue for the LTT (SR-PT) cycle with the GBC14-200 power turbine at pressure ratios less than 1.41.

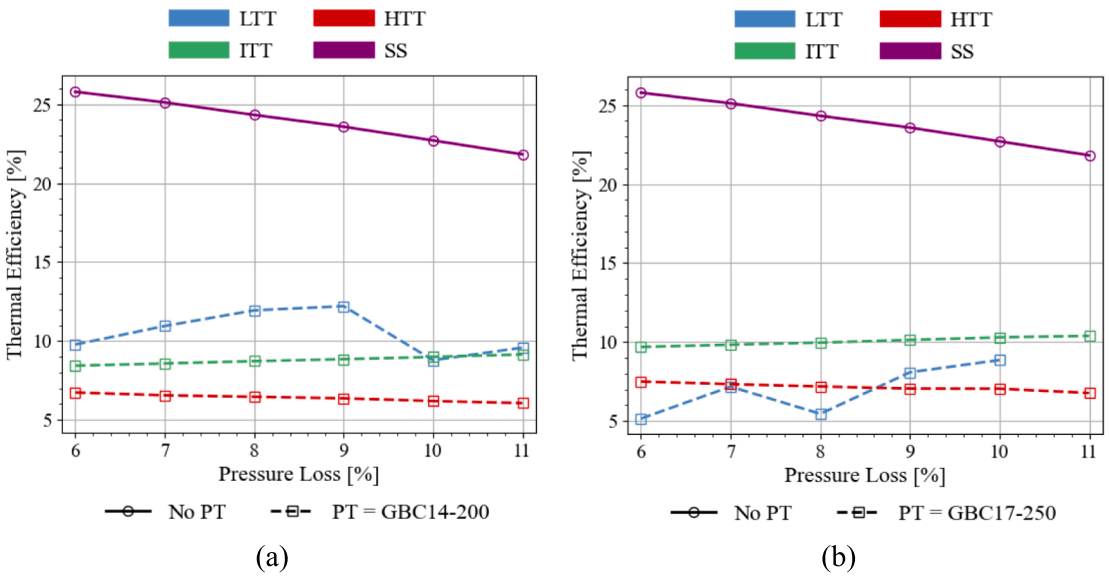

Fig. 13. Thermal efficiency as a function of pressure loss for the G25-550 (AR = 0.92) as the GT in a recuperated cycle at a compressor pressure ratio of 1.8 with (a) the GBC14-200 as the PT and (b) the GBC17-250 as the PT.

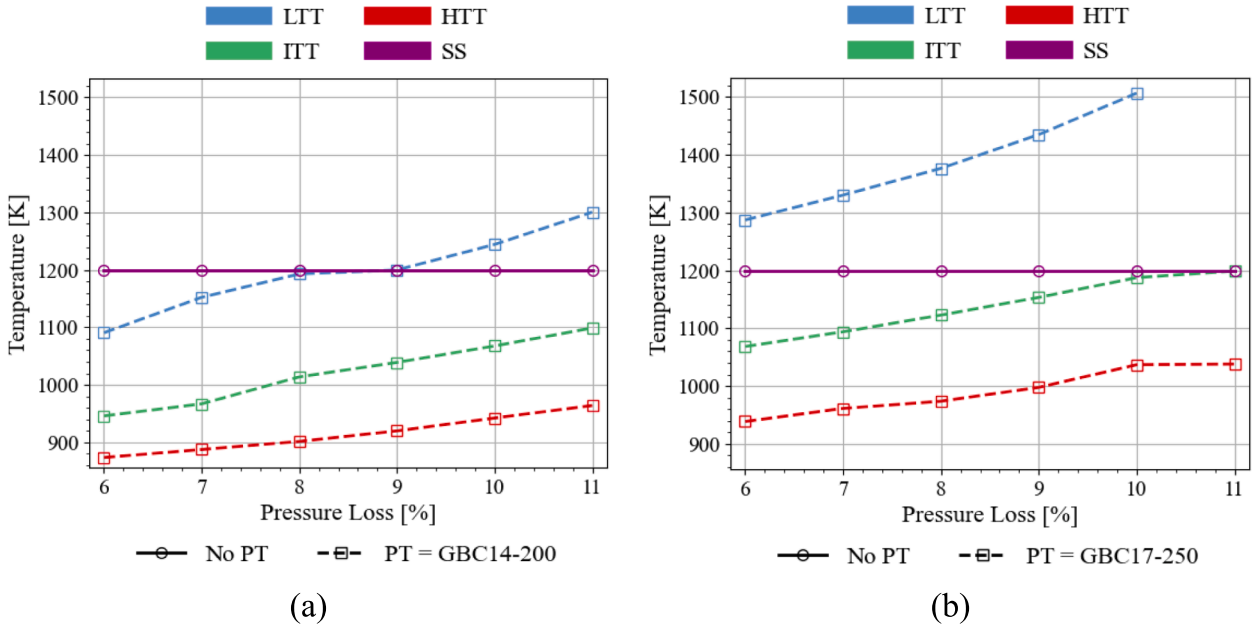

Fig. 14. GT inlet temperature as a function of pressure loss for the G25-550 (AR = 0.92) as the GT in a recuperated cycle at a compressor pressure ratio of 1.8 with (a) the GBC14-200 as the PT and (b) the GBC17-250 as the PT.

For the GTX4088R (AR = 1.19) main shaft turbocharger, the HTT (SR-CC) cycle with the GBC17-250 power turbine produces the overall greatest thermal efficiency of all the cycles, as shown in Fig. 15(d), at high pressure ratios. This maximum performance obtains a power output of 15.3 kW (see Fig. B5) and a thermal efficiency of 4.49 % at a pressure ratio of 2.75, due to exceeding the gasifier turbine inlet temperature limit at pressure ratios greater than 2.75. The single-shaft cycle has a power output of 11.3 kW (see Fig. B5) and a thermal efficiency of 4.05 % at a pressure ratio of 3. At a pressure ratio of 2.5, the HTT (SR-CC) cycle with the GBC17-250 power turbine has a power output of 12.3 kW (shown in Fig. B5) and a thermal efficiency of 4.01 % (shown in Fig. 15(d)), with the single-shaft cycle obtaining a power output of 8.9 kW (see Fig. B5) and a thermal efficiency of 3.69 % at the same pressure ratio. Fig. 16 shows that gasifier turbine inlet temperatures that exceed 1200 K are only limiting for the LTT (SR-PT) and HTT (SR-CC) cycles with the GBC17-250 as the power turbine at low pressure ratios, and for the LTT (SR-CC) and ITT(S) (SR-CC) cycles for both power turbine options. The remaining temperature limitations, consisting of the power turbine inlet temperatures and the maximum solar receiver surface temperatures are within the allowable limit for all the cycles. Additionally, the HTT (SR-CC) cycle with the GBC17-250 power turbine has slightly too high gasifier and power turbine inlet temperatures at pressure ratios less than 1.75, as shown in Fig. 16 with the gasifier turbine and power turbine inlet temperatures being the same for the HTT (SR-CC) configuration. This is however not in the operational region where this cycle obtains the best performance and thus is not of major concern.

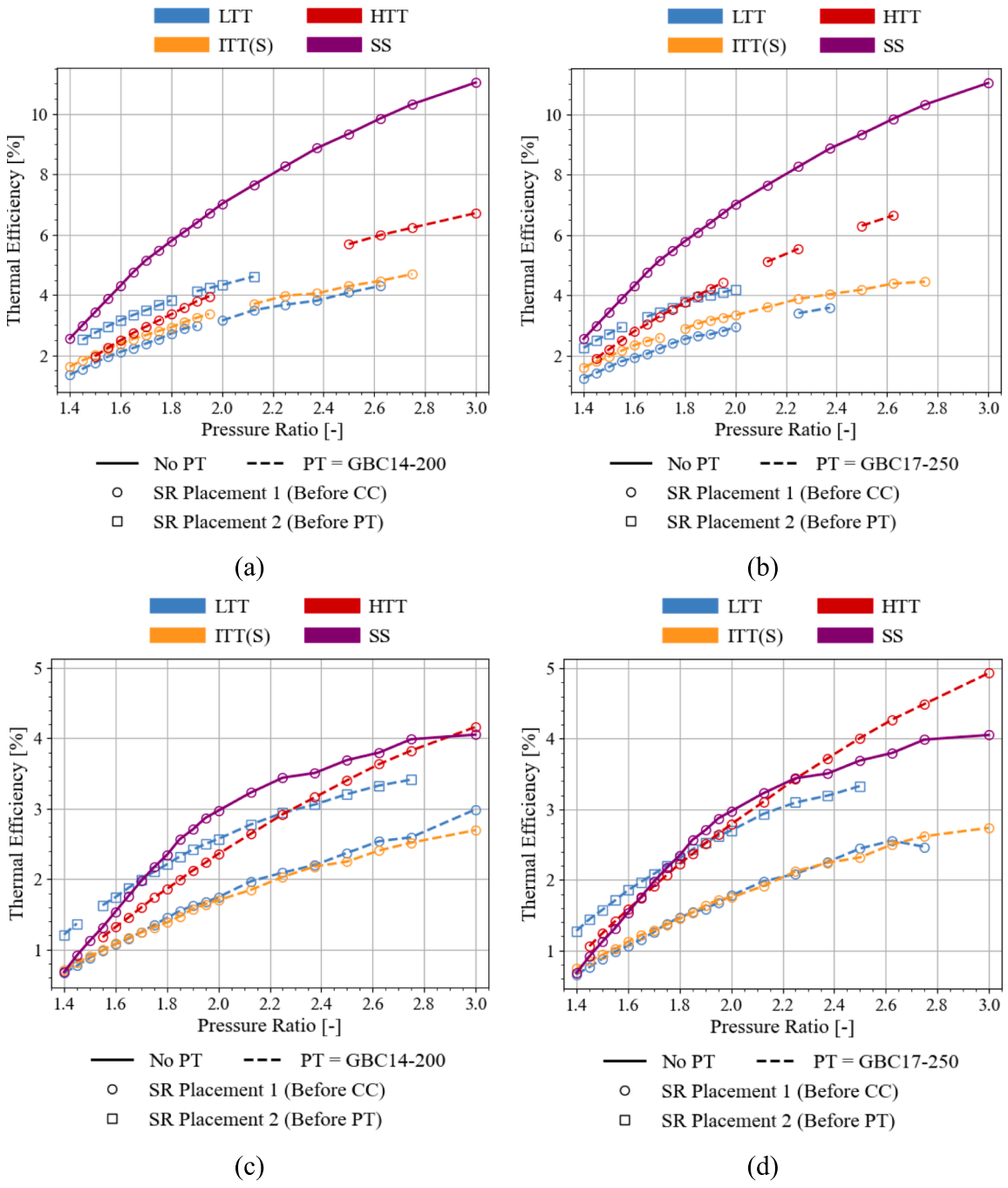

Fig. 15. Thermal efficiency as a function of pressure ratio in a simple solar cycle for (a) the G25-550 (AR = 0.92) as the GT and GBC14-200 as the PT, (b) the G25-550 (AR = 0.92) as the GT and GBC17-250 as the PT, (c) the GTX4088R (AR = 1.19) as the GT and GBC14-200 as the PT, and (d) the GTX4088R (AR = 1.19) as the GT and GBC17-250 as the PT (adapted from Cockcroft & Le Roux [19]).

3.3.1. Effect of pressure drop on the simple solar cycle results

When it comes to increased cycle pressure losses, Fig. 17 shows that the thermal efficiency response of the LTT (SR-CC) and LTT (SR-PT) cycles is the same as that of the simple LTT cycle, the response of the HTT (SR-CC) cycle is the same as that of the simple HTT cycle, and response of the simple solar single-shaft cycle is the same the simple single-shaft cycle.

In terms of comparative performance, the LTT (SR-PT) cycle with the GBC17-250 as the power turbine gets close to the thermal efficiency of the single-shaft cycle at a pressure loss of 11 %. However, at this high pressure loss percentage the gasifier turbine inlet temperature is too high and is expected to increase under even greater pressure losses, as shown in Fig. 18. High gasifier turbine inlet temperatures are also of concern for the LTT (SR-CC) and ITT(S) (SR-CC) cycles, for both power turbine options, as shown in Fig. 18. The power turbine inlet temperatures and the maximum solar receiver surface temperatures were all found to be within the limit of 1200 K, for each cycle configuration. For simplicity, these results are not included in this section. Considering the discussions in this section, none of the parallel-flow cycles offer a performance advantage over the single-shaft cycle in a simple solar cycle when the G25-550 (AR = 0.92) is used as the main shaft turbocharger, even under greater pressure loss considerations.

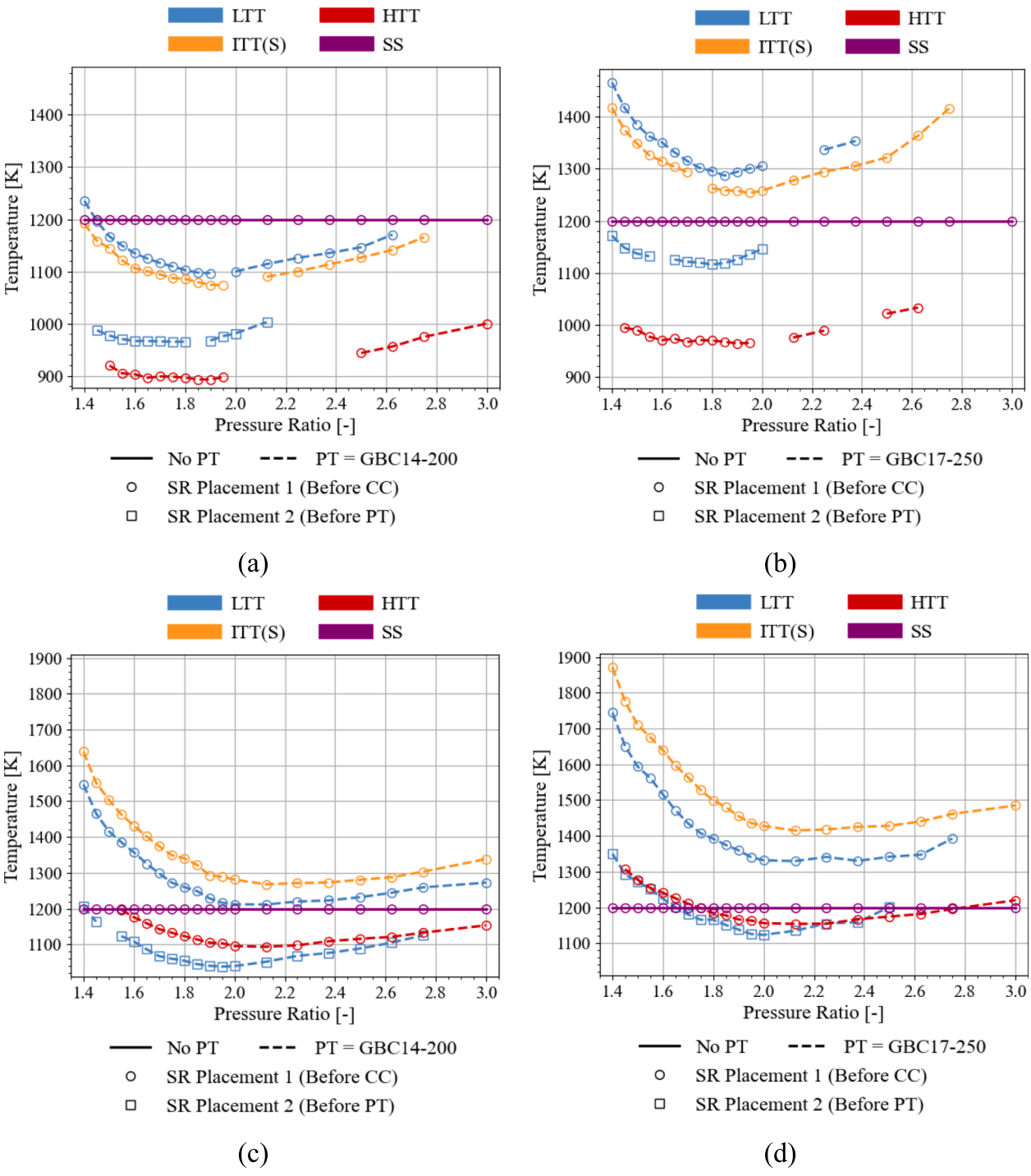

Fig. 16. GT inlet temperature as a function of pressure ratio in a simple solar cycle for (a) the G25-550 (AR = 0.92) as the GT and GBC14-200 as the PT, (b) the G25-550 (AR = 0.92) as the GT and GBC17-250 as the PT, (c) the GTX4088R (AR = 1.19) as the GT and GBC14-200 as the PT, and (d) the GTX4088R (AR = 1.19) as the GT and GBC17-250 as the PT (adapted from Cockcroft & Le Roux [19]).

3.4. Recuperated solar cycle results

When comparing thermal efficiencies, for the G25-550 (AR = 0.92) main shaft turbocharger, Fig. 19(a) shows that when the GBC14-200 is used as the power turbine, the LTT (SR-PT) cycle has its highest thermal efficiency, of 17.68 %, at a pressure ratio of 1.5, while remaining within all the temperature limitations for its entire operational range (as shown in Fig. 20(a), Fig. 21(a), Fig. 22(a)). Due to high solar receiver surface temperatures, as shown in Fig. 22, the single-shaft cycle is only operable at pressure ratios greater than 1.75, with a thermal efficiency of 21.8 % at this pressure ratio, and the LTT (SR-CC) cycle with the GBC14-200 power turbine is only operable at pressure ratios greater than 1.9, with a thermal efficiency of 15.4 % at this pressure ratio. When the GBC17-250 is used as the power turbine at a pressure ratio of 1.6, the LTT (SR-PT) cycle obtains a thermal efficiency of 23.51 %, as shown in Fig. 19(b), with a power output of 3 kW (shown in Fig. B7(b)), while remaining within all the temperature limitations (as shown in Fig. 20(b), Fig. 21(b), Fig. 22(b)). This configuration and combination is however not recommended for operation at pressure ratios of greater than 1.95 due to exceeding the maximum allowable gasifier turbine inlet

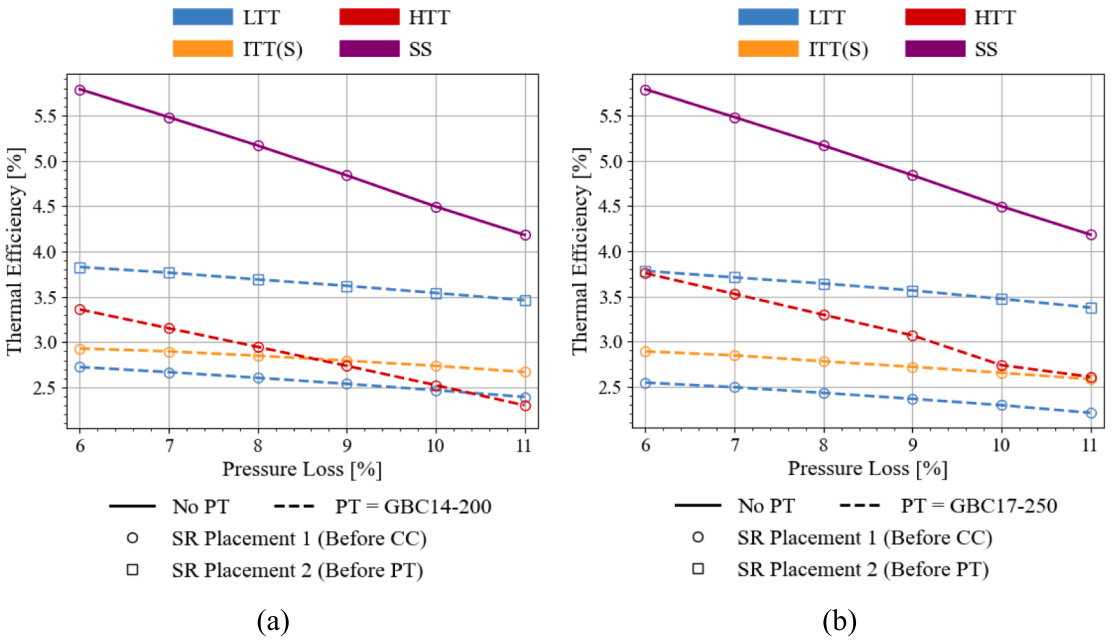

Fig. 17. Thermal efficiency as a function of pressure loss for the G25-550 (AR = 0.92) as the GT in a simple solar cycle at a compressor pressure ratio of 1.8 with (a) the GBC14-200 as the PT and (b) the GBC17-250 as the PT.

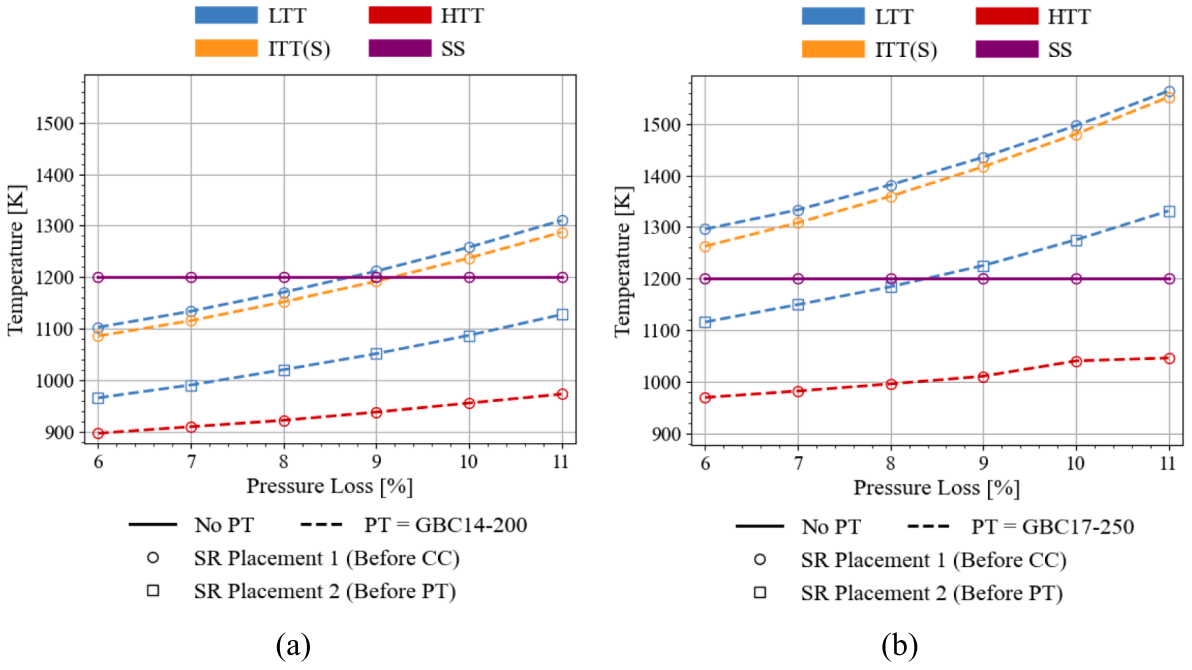

Fig. 18. GT inlet temperature as a function of pressure loss for the G25-550 (AR = 0.92) as the GT in a simple solar cycle at a compressor pressure ratio of 1.8 with (a) the GBC14-200 as the PT and (b) the GBC17-250 as the PT.

temperature of 1200 K (as shown in Fig. 20(b)).

When the GTX4088R (AR = 1.19) acts as the main shaft turbocharger in a recuperated solar cycle, Fig. 19 shows that the overall best thermal efficiency is obtained in the operation of the LTT (SR-PT) cycle, when both the GBC14-200 and the GBC17-250 are considered as power turbine options. Both of these cycles fully outperform the single-shaft cycle, with all of the parallel-flow cycles utilising the 'SR-PT' receiver placement allowing for better thermal efficiency performance than the single-shaft cycle. However, Fig. 20 shows that at this pressure ratio, the gasifier turbine inlet temperature is too high for this configuration with the GBC17-250 power turbine, with the cycle only being feasible for operation pressure ratios between 1.84 and 2.3 with thermal efficiencies from 8.19 % to 7.63 %, respectively, as per Fig. 19(d), and power outputs between 4.5 kW and 7.6 kW (see Fig. B7). For the GTX4088R (AR = 1.19) main shaft turbocharger, when the LTT (SR-PT) configuration is used with the GBC14-200 as the power turbine, none of the temperature limits are exceeded (as shown in Fig. 20(c), Fig. 21(c), Fig. 22(c)) and thus the cycle is feasible for operation throughout the simulated pressure ratio range. This, LTT (SR-PT) configuration with the GBC14-200 power turbine, has an overall maximum thermal efficiency of 9.09 % with a power output of 2.6 kW (see Fig. B7), at a pressure ratio of 1.5. This is the highest feasible thermal efficiency when the GTX4088R (AR = 1.19)

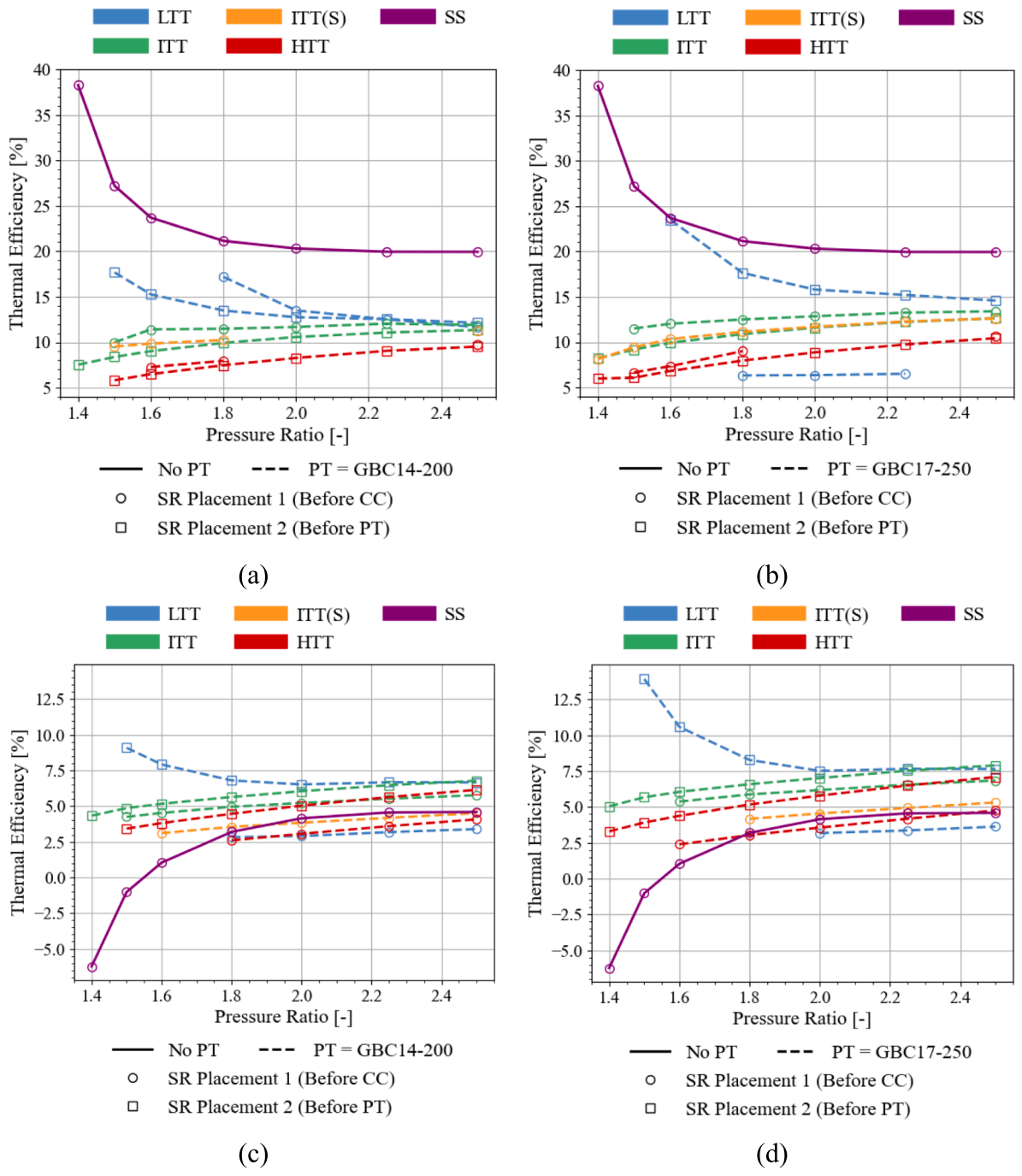

Fig. 19. Thermal efficiency as a function of pressure ratio in a recuperated solar cycle for (a) the G25-550 (AR = 0.92) as the GT and GBC14-200 as the PT, (b) the G25-550 (AR = 0.92) as the GT and GBC17-250 as the PT, (c) the GTX4088R (AR = 1.19) as the GT and GBC14-200 as the PT, and (d) the GTX4088R (AR = 1.19) as the GT and GBC17-250 as the PT (adapted from Cockcroft & Le Roux [19]).

is used as the main shaft turbocharger for the considered configurations and combinations.

3.4.1. Effect of pressure drop on the recuperated solar cycle results

For greater pressure loss percentages, Fig. 23 shows that the LTT (SR-PT) cycle with the GBC14-200 as the power turbine is the only viable cycle for achieving a greater thermal efficiency than the single-shaft cycle at pressure losses exceeding 8.7 %, with increasing thermal efficiency values between 13.5 % and 19.9 % for pressure losses between 6 % and 11 %, for a constant power output of approximately 3.6 kW (see Fig. B8) for all the pressure losses, at a pressure ratio of 1.8. This is achievable while remaining within the maximum allowable solar receiver surface temperature, as shown in Fig. 25 (a). The thermal efficiency of the single-shaft cycle declines from 21.8 % to 12.7 % at a pressure ratio of 1.8. Thus, for high combustion chamber pressure losses, LTT (SR-PT) cycle with the GBC14-200 as the power turbine is the best cycle configuration. The LTT (SR-PT) configuration with the GBC17-250 as the power turbine has high gasifier turbine inlet temperatures at higher pressure losses, as shown in Fig. 24. These high gasifier turbine inlet temperatures result in poorer performing geometry selections (as per Appendix A) to remain within, or as close as possible to, the allowable maximum gasifier turbine inlet temperature of 1200 K. The power turbine inlet temperatures were found to be within range (below 1200 K) for all the considered cycles.

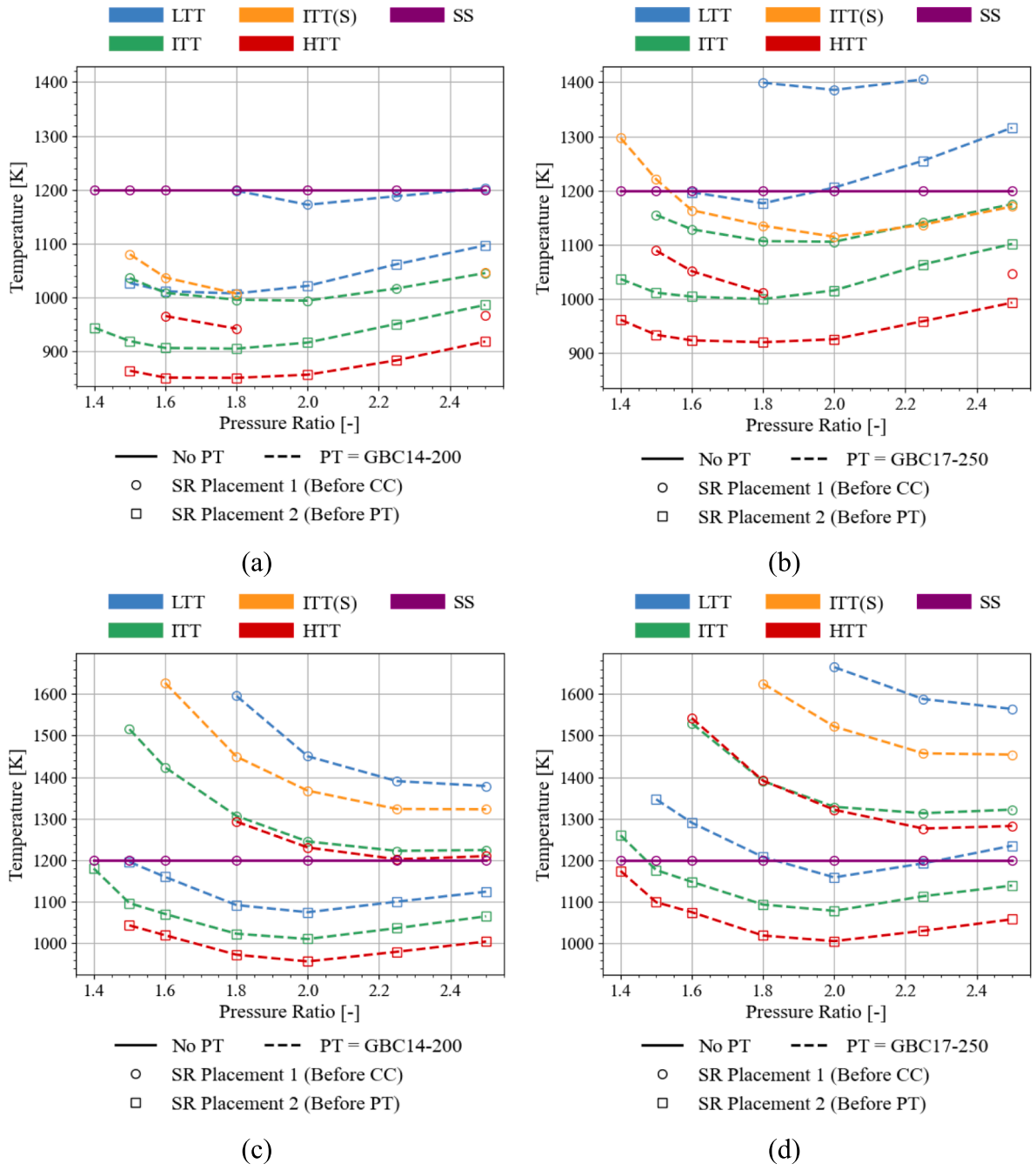

Fig. 20. GT inlet temperature as a function of pressure ratio in a recuperated solar cycle for (a) the G25-550 (AR = 0.92) as the GT and GBC14-200 as the PT, (b) the G25-550 (AR = 0.92) as the GT and GBC17-250 as the PT, (c) the GTX4088R (AR = 1.19) as the GT and GBC14-200 as the PT, and (d) the GTX4088R (AR = 1.19) as the GT and GBC17-250 as the PT (adapted from Cockcroft & Le Roux [19]).

3.5. Summary of results

The thermal efficiency of the various cycles is important when it comes to addressing the output that is obtainable with reference to the fuel added to the cycle, with a higher thermal efficiency indicating a better proportional usage of the cycle fuel input. The results for obtaining the maximum thermal efficiency for each of the different main shaft turbochargers in each cycle type, are shown in Table 1 (for a combustion pressure loss of 6 % only). This table shows that the cycles consisting of the larger GTX4088R (AR = 1.19) main shaft turbocharger always offer better thermal efficiency than the G25-550 (AR = 0.92) when a parallel-flow cycle is identified as the best configuration, except in a recuperated solar cycle. Furthermore, the table shows the effect of pressure loss on a single-shaft cycle, where the feasibility of a parallel-flow cycle increases when more pressure loss components are used.

Overall, the best cycle for achieving the highest thermal efficiency, when the combustion chamber pressure loss is 6 % of the incoming combustion pressure, is the recuperated single-shaft cycle with the G25-550 (AR = 0.92) as the main shaft turbocharger. This cycle does however experience greater performance reductions than other cycles when cycle pressure losses increase. The second-best cycle, when the combustion chamber pressure loss is 6 % of the incoming combustion pressure, is the recuperated solar LTT (SR-PT) cycle with the G25-550 (AR = 0.92) as the main shaft turbocharger and the GBC17-250 as the power turbine. However, when greater pressure losses, of up to 11 %, are considered, as expected for an experimentally implemented cycle, the

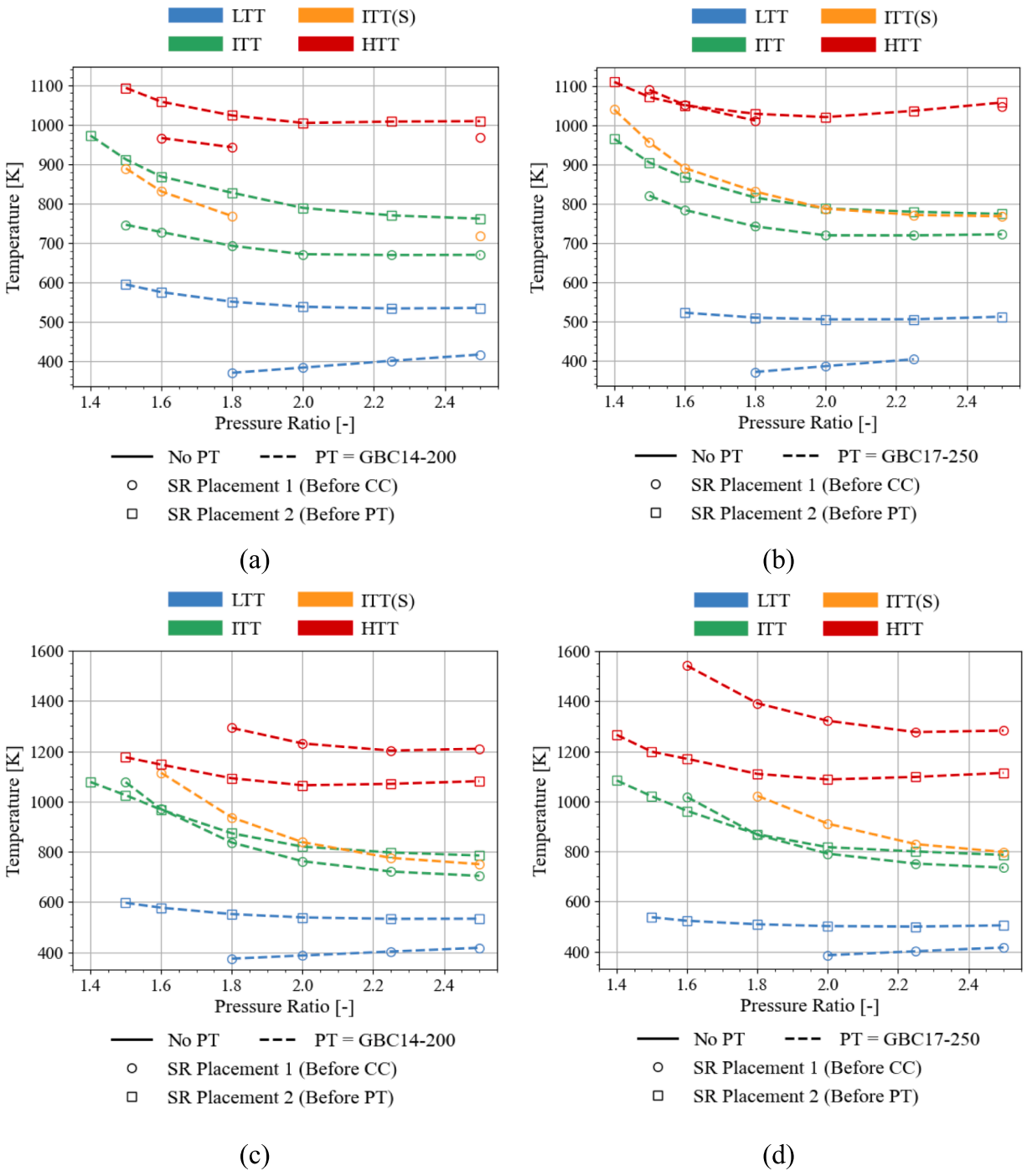

Fig. 21. PT inlet temperature as a function of pressure ratio in a recuperated solar cycle for (a) the G25-550 (AR = 0.92) as the GT and GBC14-200 as the PT, (b) the G25-550 (AR = 0.92) as the GT and GBC17-250 as the PT, (c) the GTX4088R (AR = 1.19) as the GT and GBC14-200 as the PT, and (d) the GTX4088R (AR = 1.19) as the GT and GBC17-250 as the PT (adapted from Cockcroft & Le Roux [19]).

GBC14-200 needs to be used as the power turbine to allow for good thermal efficiency and power output performance, while not exceeding the maximum allowable gasifier turbine inlet temperature. This allows for thermal efficiencies of between 13.5 % and 19.9 % (see Fig. 23), with a constant power output of approximately 3.6 kW (see Fig. B8), for pressure loss percentages of between 6 % and 11 % at a pressure ratio of 1.8. In addition to an increase in thermal efficiency with an increase in pressure loss, the recuperated solar LTT (SR-PT) cycle with the GBC14-200 as the power turbine fully outperforms the thermal efficiency of its single-shaft counterpart, at a pressure ratio of 1.8, for combustion chamber pressure loss percentages exceeding 8.7 %. This means that this cycle – the recuperated solar LTT (SR-PT) cycle with the G25-550 (AR = 0.92) as the main shaft turbocharger and the GBC14-200 as the power turbine – is expected to outperform the single-shaft cycle at the experimental pressure loss percentage of 10.2 % as determined by Swanepoel et al. [18].

4. Conclusion

In this study, various parallel-flow Brayton cycle configurations, developed from turbochargers, were compared to their single-shaft counterparts. The effects of adding pressure-drop components

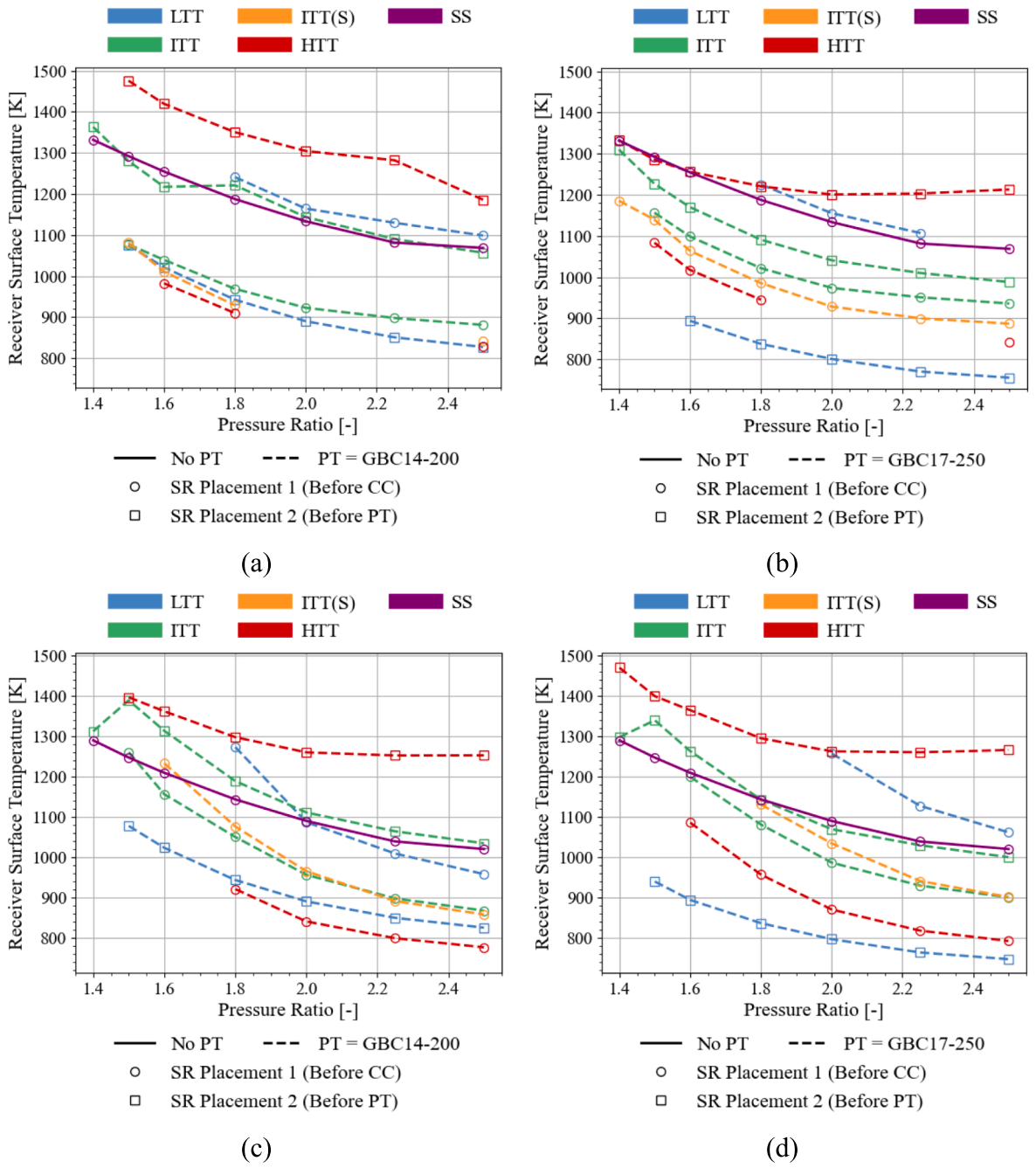

Fig. 22. Maximum solar receiver surface temperature as a function of pressure ratio in a recuperated solar cycle for (a) the G25-550 (AR = 0.92) as the GT and GBC14-200 as the PT, (b) the G25-550 (AR = 0.92) as the GT and GBC17-250 as the PT, (c) the GTX4088R (AR = 1.19) as the GT and GBC14-200 as the PT, and (d) the GTX4088R (AR = 1.19) as the GT and GBC17-250 as the PT (adapted from Cockcroft & Le Roux [19]).

(combustion chamber, recuperator and solar receiver) were considered. The solar receiver dimensions were fixed while the recuperator dimensions were variables that were optimised. Combustion chamber pressure losses were investigated from 6 % to 11 %. Furthermore, turbine inlet temperatures and solar receiver surface temperatures were constrained to 1200 K. The larger GTX4088R (AR = 1.19) main shaft turbocharger almost always offered the best cycle performance when a parallel-flow cycle was identified as the most efficient. When assuming a combustion chamber pressure loss of 6 %, the high-temperature turbine (HTT) cycle was identified as the best simple cycle, the single-shaft cycle was the best recuperated cycle, and the HTT (with the solar receiver before the combustion chamber) was the best simple solar cycle. However, when the G25-550 (AR = 0.92) was used as the main shaft turbocharger, the single-shaft cycle offered the best thermal efficiency for the simple, recuperated, and simple solar cycles. The overall highest thermal efficiency, when assuming a combustion chamber pressure loss of 6 %, was obtained for the G25-550 (AR = 0.92) turbocharger in a recuperated single-shaft cycle. However, the thermal efficiencies of single-shaft cycles showed a significant decline with an increase in cycle pressure losses.

For a recuperated solar cycle, the best cycle configuration for obtaining the maximum cycle thermal efficiency was the parallel-flow LTT cycle with the solar receiver before the power turbine (SR-PT). When the GTX4088R (AR = 1.19) was used as the main shaft turbocharger, the mentioned configuration with the GBC14-200 as the power turbine offered a best-case thermal efficiency of 9.1 % (with 2.6 kW of power output) at a pressure ratio of 1.5. When the G25-550 (AR = 0.92) was used as the main shaft turbocharger, the same configuration with

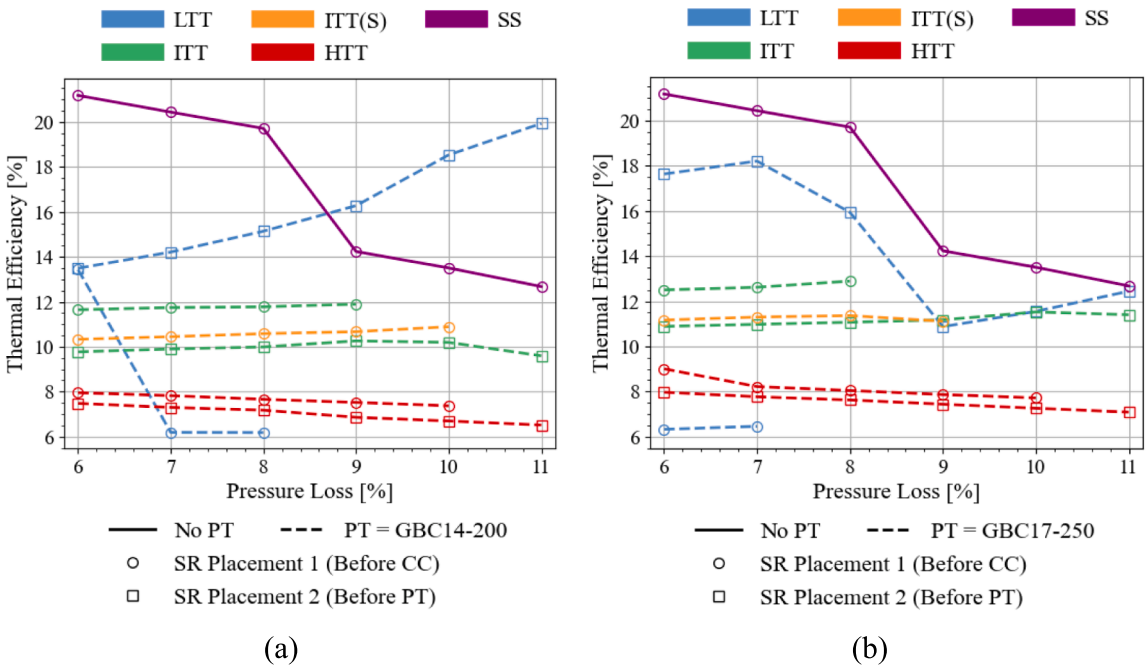

Fig. 23. Thermal efficiency as a function of pressure loss for the G25-550 (AR = 0.92) as the GT in a recuperated solar cycle at a compressor pressure ratio of 1.8 with (a) the GBC14-200 as the PT and (b) the GBC17-250 as the PT.

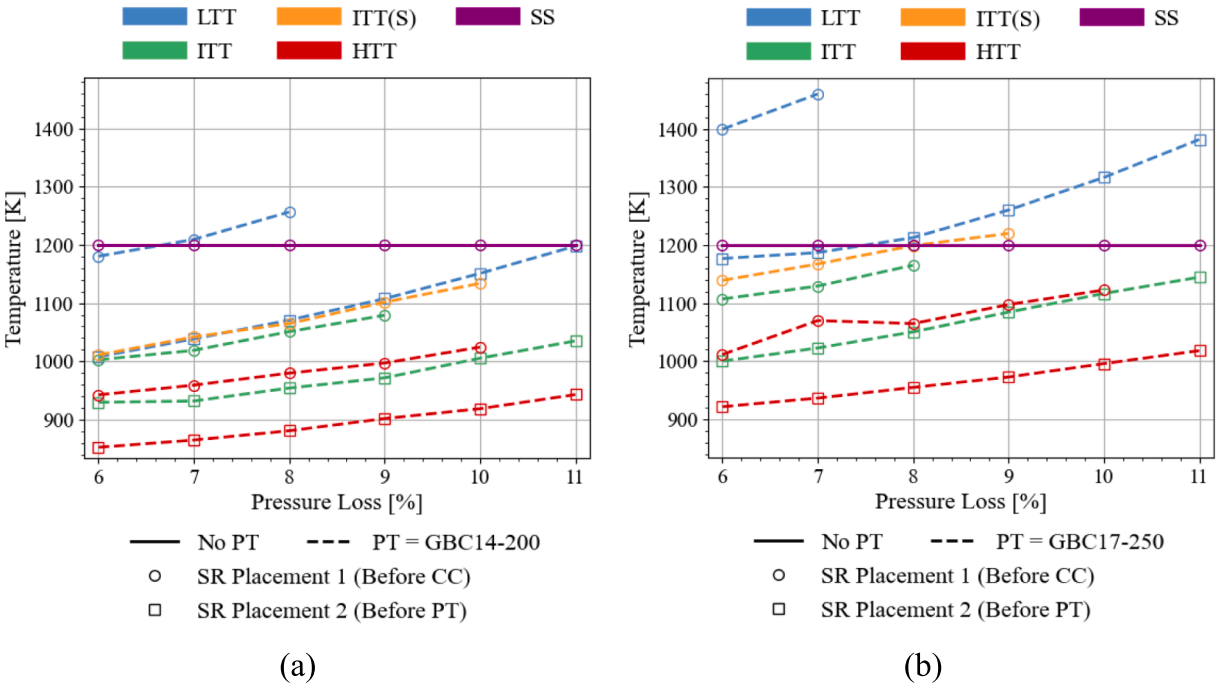

Fig. 24. GT inlet temperature as a function of pressure loss for the G25-550 (AR = 0.92) as the GT in a recuperated solar cycle at a compressor pressure ratio of 1.8 with (a) the GBC14-200 as the PT and (b) the GBC17-250 as the PT.

the GBC17-250 as the power turbine offered a best-case thermal efficiency of 23.5 % (with 3 kW of power output) at a pressure ratio of 1.6.

Under greater combustion pressure loss considerations, for the G25-550 (AR = 0.92) as the main shaft turbocharger, results showed that the recuperated solar LTT (SR-PT) cycle would still offer the highest recuperated solar cycle thermal efficiencies. However, the GBC14-200 should be selected over the GBC17-250 as the power turbine to prevent gasifier turbine inlet temperatures that exceed 1200 K. The recuperated solar LTT (SR-PT) cycle with the GBC14-200 as the power turbine offers the highest thermal efficiency range at pressure losses of between 6 % and 11 % with increasing thermal efficiencies of 13.5 % to 19.9 % and a constant power output of 3.6 kW at a pressure ratio of 1.8. At this pressure ratio, the recuperated solar LTT (SR-PT) cycle with the GBC14-200 as the power turbine outperforms the single-shaft cycle at combustion chamber pressure loss percentages greater than 8.7 %.

4.1. Recommendations

It is recommended that for the implementation of a parallel-flow experimental solar Brayton cycle, the recuperated solar LTT (SR-PT)

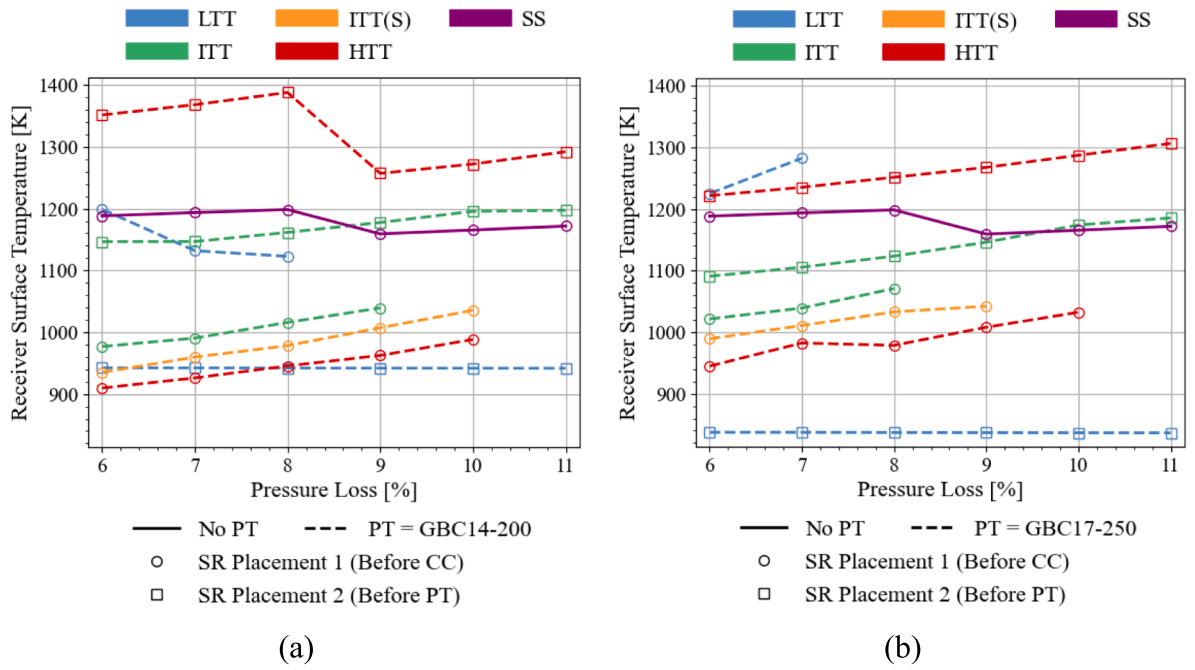

Fig. 25. Maximum solar receiver surface temperature as a function of pressure loss for the G25-550 (AR = 0.92) as the GT in a recuperated solar cycle at a compressor pressure ratio of 1.8 with (a) the GBC14-200 as the PT and (b) the GBC17-250 as the PT.

Table 1
Summary of the best configuration and combination for each cycle type to obtain the maximum thermal efficiency for a combustion pressure loss of 6%.

Cycle Type	Gasifier Turbocharger	Best Configuration	Best Power Turbine	Pressure Ratio for Maximum η_{th} [-]	Maximum η_{th} [%]
Simple	G25-550 (AR = 0.92)	SS	–	2.5	8.8
	GTX4088R (AR = 1.19)	HTT	GBC17-250	2.5	4.5
Recuperated	G25-550 (AR = 0.92)	SS	–	1.5	45.4
	GTX4088R (AR = 1.19)	SS	–	2.0	8.4
Simple Solar	G25-550 (AR = 0.92)	SS	–	3.0	11.0
	GTX4088R (AR = 1.19)	HTT (SR-CC)	GBC17-250	2.75	4.5
Recuperated Solar	G25-550 (AR = 0.92)	LTT (SR-PT)	GBC17-250	1.6	23.5
	GTX4088R (AR = 1.19)	LTT (SR-PT)	GBC14-200	1.5	9.1

cycle with the G25-550 (AR = 0.92) main shaft turbocharger and the GBC14-200 power turbine should be used due to its high thermal efficiencies and constant power output under greater pressure loss considerations. This cycle is expected to operate well at various pressure ratios and pressure losses while not exceeding the cycle temperature limitations. Additionally, this cycle operates best at low pressure ratios, which allows for an extended turbomachinery operational lifespan (due to the low pressure ratio application) and lower cycle running costs as a result of the higher thermal efficiency (and subsequent lower reliance on the combustion of LPG). However, for a simpler non-solar cycle, the recuperated single-shaft cycle with the G25-550 (AR = 0.92) main shaft turbocharger can offer better thermal efficiency performance when combustion chamber pressure losses are low, and can therefore also be used for implementation.

To further investigate the application of the recuperated solar LTT (SR-PT) cycle it is recommended to implement an experimental study to ascertain the viability of the cycle for reducing energy consumption. This study can also be used to validate the analytical results of the current study. Moreover, an analytical study can be done to investigate the influence of utilising two solar receivers for the various cycle configurations, to make use of both the 'SR-CC' dish placement and the 'SR-PT' dish placement to further ascertain the extent of cycle performance improvement that can be obtained with the utilisation of both receiver placements.

CRediT authorship contribution statement

C.C. Cockcroft: Writing – original draft, Visualization, Software, Methodology, Investigation, Formal analysis, Data curation, Conceptualization. **W.G. Le Roux:** Writing – review & editing, Supervision, Resources, Project administration, Methodology, Funding acquisition, Conceptualization.

Declaration of competing interest

The authors declare that they have no known competing financial interests or personal relationships that could have appeared to influence the work reported in this paper.

Acknowledgements

The authors would like to thank the Department of Science and Innovation (DSI) for their financial support to the UP Solar Thermal Spoke through the Renewable Energy Hub and Spokes Programme.

Appendix A. Best recuperator dimensions for each recuperated configuration

The recuperator dimensions used to generate the results for each cycle configuration that uses a recuperator is summarised in this section. This recuperator is illustrated in Fig. A1.

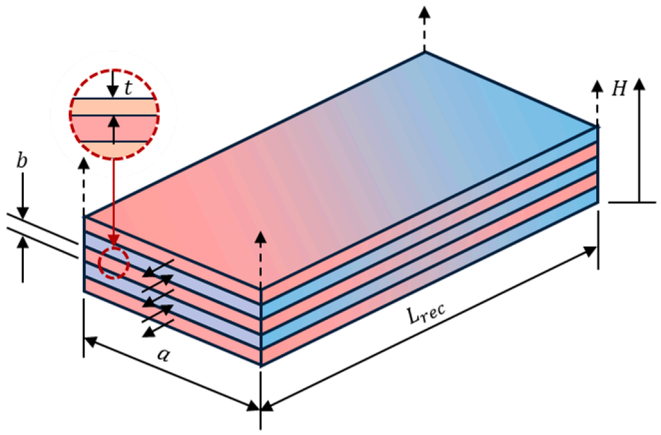

Fig. A1. Recuperator structure and dimensions as adapted from Cockcroft & Le Roux [19,23].

Table A1 shows the best recuperator geometry over the entire pressure ratio range for each recuperated and recuperated solar cycle with the G25-550 (AR = 0.92) as the main shaft turbocharger. Table A2 shows the best recuperator geometry over the entire pressure ratio range for each recuperated cycle with the GTX4088R (AR = 1.19) as the main shaft turbocharger. The geometry selections in Tables A1 and A2 are made as a result of these recuperator geometries ensuring a maximum cycle thermal efficiency, under the consideration of the entire pressure ratio range, while not exceeding the maximum allowable gasifier turbine inlet temperature of 1200 K. Tables A3 and A4 are generated in a similar manner, but for different combustion chamber pressure losses for the recuperated and recuperated solar cycles, respectively, for the G25-550 (AR = 0.92) main shaft turbocharger. However, for the generation of Tables A3 and A4, the best-case geometry at each pressure loss percentage is selected for each configuration, instead of considering the entire pressure loss range. This is why some of the pressure loss profiles in the results section have abrupt behavioural characteristics, as the recuperator geometry changes to accommodate the maximum thermal efficiency, under the consideration of the various temperature limitations (including the receiver surface temperature limitation. For many of the single-shaft cycles, no results are obtained when higher amounts of recuperator channels are used. This is why the single-shaft results often make use of fewer channels.

Table A1
Recuperator dimensions used for each recuperated and recuperated solar configuration for different PT options with the G25-550 (AR = 0.92) as the GT considering the entire pressure ratio range.

Power Turbine	Cycle Type	Cycle Configuration	Number of Channels [-]	Channel Height [mm]
GBC14-200	Recuperated	SS	45.0	3.00
		LTT	45.0	1.50
		ITT	45.0	2.25
		HTT	45.0	1.50
	Recuperated Solar	SS	30.0	4.50
		LTT (SR-CC)	45.0	2.25
		LTT (SR-PT)	45.0	1.50
		ITT (SR-CC)	45.0	3.75
		ITT (SR-PT)	45.0	3.00
		ITT(S) (SR-CC)	45.0	3.00
		HTT (SR-CC)	45.0	2.25
		HTT (SR-PT)	45.0	3.75
GBC17-250	Recuperated	SS	45.0	3.00
		LTT	22.5	4.50
		ITT	45.0	1.50
		HTT	45.0	3.75
	Recuperated Solar	SS	30.0	4.50
		LTT (SR-CC)	15.0	4.50
		LTT (SR-PT)	45.0	1.50
		ITT (SR-CC)	45.0	2.25
		ITT (SR-PT)	45.0	3.00
		ITT(S) (SR-CC)	45.0	3.00
		HTT (SR-CC)	45.0	3.00
		HTT (SR-PT)	45.0	3.75

Table A2
Recuperator dimensions used for each recuperated and recuperated solar configuration for different PT options with the GTX4088R (AR = 1.19) as the GT considering the entire pressure ratio range.

Power Turbine	Cycle Type	Cycle Configuration	Number of Channels [-]	Channel Height [mm]
GBC14-200	Recuperated	SS	45.0	4.50
		LTT	45.0	2.25
		ITT	45.0	4.50
		HTT	45.0	4.50
	Recuperated Solar	SS	37.5	4.50
		LTT (SR-CC)	15.0	4.50
		LTT (SR-PT)	45.0	3.00
		ITT (SR-CC)	30.0	4.50
		ITT (SR-PT)	45.0	3.00
		ITT(S) (SR-CC)	22.5	4.50
		HTT (SR-CC)	15.0	4.50
		HTT (SR-PT)	45.0	4.50
GBC17-250	Recuperated	SS	45.0	4.50
		LTT	37.5	4.50
		ITT	45.0	3.00
		HTT	45.0	3.75
	Recuperated Solar	SS	37.5	4.50
		LTT (SR-CC)	15.0	4.50
		LTT (SR-PT)	45.0	3.75
		ITT (SR-CC)	30.0	4.50
		ITT (SR-PT)	45.0	3.00
		ITT(S) (SR-CC)	22.5	4.50
		HTT (SR-CC)	15.0	4.50
		HTT (SR-PT)	45.0	4.50

Table A3
Recuperator dimensions used for each recuperated configuration for different PT options with the G25-550 (AR = 0.92) as the GT considering different combustion chamber pressure losses.

Power Turbine	Cycle	Combustion Chamber Pressure Loss [%]					
		6 %	7 %	8 %	9 %	10 %	11 %
Channel Height [mm]							
–	SS	3.00	3.00	3.00	3.00	3.00	3.00
GBC14-200	LTT	2.25	1.50	1.50	3.00	4.50	4.50
	ITT	3.00	3.00	1.50	1.50	1.50	1.50
	HTT	3.00	3.00	3.75	3.00	2.25	2.25
GBC17-250	LTT	4.50	4.50	4.50	4.50	4.50	–
	ITT	1.50	1.50	1.50	1.50	1.50	2.25
	HTT	4.50	2.25	3.00	2.25	1.50	3.00
Number of Channels [-]							
–	SS	45.0	45.0	45.0	45.0	45.0	45.0
GBC14-200	LTT	45.0	45.0	45.0	45.0	30.0	30.0
	ITT	45.0	45.0	45.0	45.0	45.0	45.0
	HTT	45.0	45.0	45.0	45.0	45.0	45.0
GBC17-250	LTT	15.0	22.5	15.0	22.5	22.5	–
	ITT	45.0	45.0	45.0	45.0	45.0	45.0
	HTT	45.0	45.0	45.0	45.0	45.0	45.0

Table A4
Recuperator dimensions used for each recuperated solar configuration for different PT options with the G25-550 (AR = 0.92) as the GT considering different combustion chamber pressure losses.

Power Turbine	Cycle	Combustion Chamber Pressure Loss [%]					
		6 %	7 %	8 %	9 %	10 %	11 %
Channel Height [mm]							
–	SS	3.75	3.75	4.50	4.50	4.50	4.50
GBC14-200	LTT (SR-CC)	4.50	4.50	4.50	–	–	–
	LTT (SR-PT)	1.50	1.50	1.50	1.50	1.50	1.50
	ITT (SR-CC)	2.25	4.50	2.25	2.25	–	–
	ITT (SR-PT)	1.50	2.25	2.25	2.25	2.25	3.00
	ITT(S) (SR-CC)	3.75	2.25	3.00	3.00	3.00	–
	HTT (SR-CC)	2.25	2.25	3.00	3.00	2.25	–
	HTT (SR-PT)	3.00	3.75	3.00	3.00	3.00	3.00
GBC17-250	LTT (SR-CC)	4.50	4.50	–	–	–	–
	LTT (SR-PT)	1.50	2.25	4.50	4.50	4.50	4.50
	ITT (SR-CC)	2.25	3.00	2.25	–	–	–
	ITT (SR-PT)	3.00	3.00	3.00	2.25	2.25	3.75
	ITT(S) (SR-CC)	2.25	3.00	3.75	3.75	–	–
	HTT (SR-CC)	3.00	1.50	3.00	2.25	2.25	–
	HTT (SR-PT)	3.00	3.75	3.00	3.75	3.00	3.00
Number of Channels [-]							
–	SS	30.0	30.0	30.0	22.5	22.5	22.5
GBC14-200	LTT (SR-CC)	37.5	15.0	15.0	–	–	–
	LTT (SR-PT)	45.0	45.0	45.0	45.0	45.0	45.0
	ITT (SR-CC)	45.0	45.0	45.0	45.0	–	–
	ITT (SR-PT)	45.0	45.0	45.0	45.0	45.0	37.5
	ITT(S) (SR-CC)	45.0	45.0	45.0	45.0	45.0	–
	HTT (SR-CC)	45.0	45.0	45.0	45.0	45.0	–
	HTT (SR-PT)	45.0	45.0	45.0	45.0	45.0	45.0
GBC17-250	LTT (SR-CC)	15.0	15.0	–	–	–	–
	LTT (SR-PT)	45.0	45.0	37.5	22.5	22.5	22.5
	ITT (SR-CC)	45.0	45.0	45.0	–	–	–
	ITT (SR-PT)	45.0	45.0	45.0	45.0	45.0	45.0
	ITT(S) (SR-CC)	45.0	45.0	45.0	45.0	–	–
	HTT (SR-CC)	45.0	45.0	45.0	45.0	45.0	–
	HTT (SR-PT)	45.0	45.0	45.0	45.0	45.0	45.0

Appendix B. Power output results of the various configurations

B.1. Simple cycle results

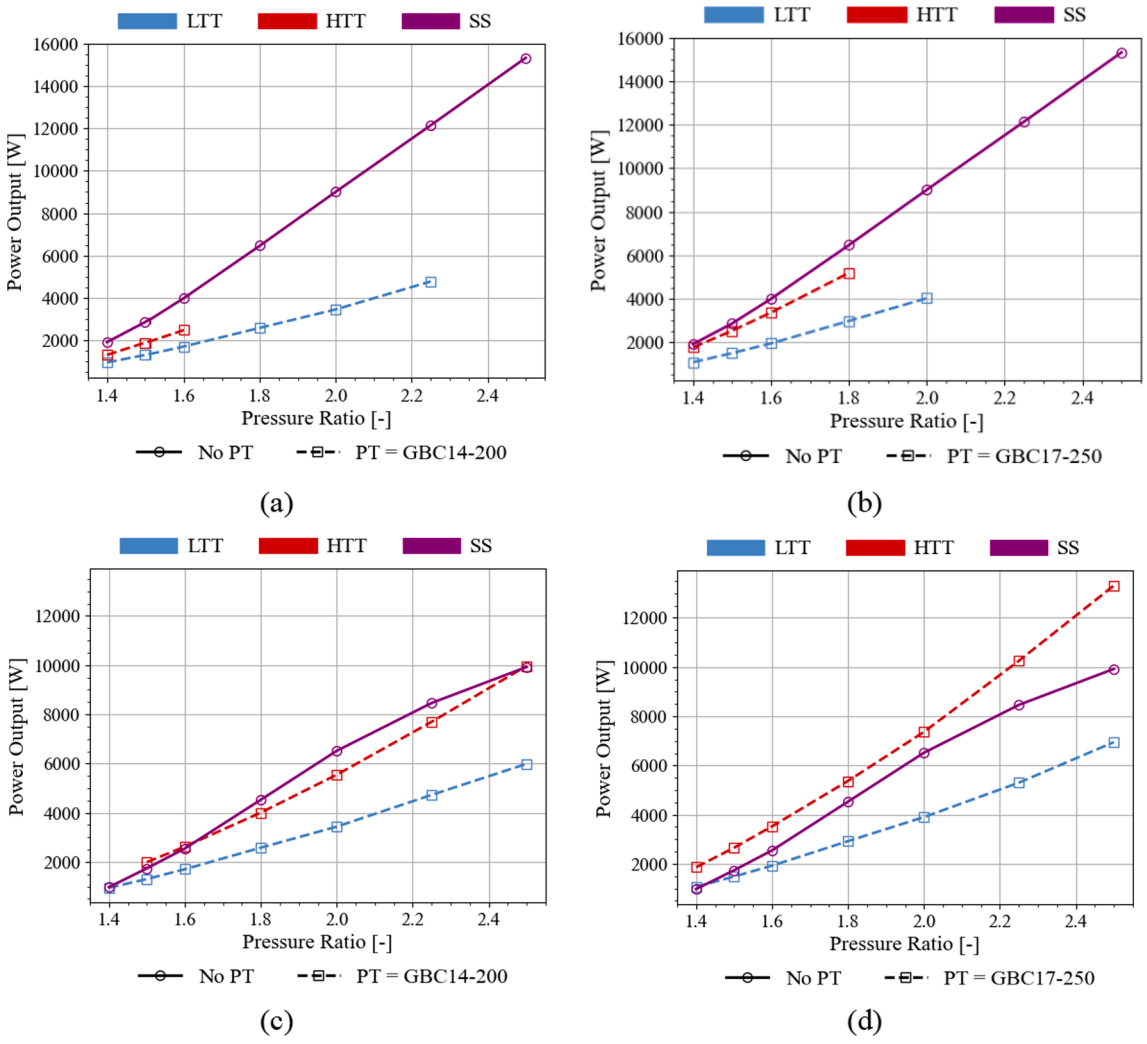

Fig. B1. Power output as a function of pressure ratio in a simple cycle for (a) the G25-550 (AR = 0.92) as the GT and GBC14-200 as the PT, (b) the G25-550 (AR = 0.92) as the GT and GBC17-250 as the PT, (c) the GTX4088R (AR = 1.19) as the GT and GBC14-200 as the PT, and (d) the GTX4088R (AR = 1.19) as the GT and GBC17-250 as the PT.

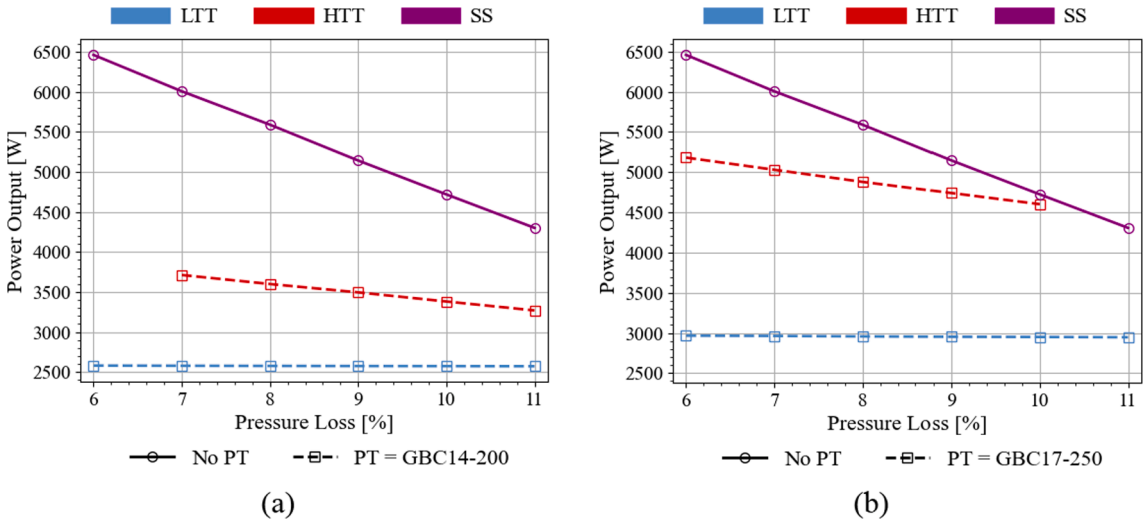

Fig. B2. Power output as a function of pressure loss for the G25-550 (AR = 0.92) as the GT in a simple cycle at a compressor pressure ratio of 1.8 with (a) the GBC14-200 as the PT and (b) the GBC17-250 as the PT.

B.2. Recuperated cycle results.

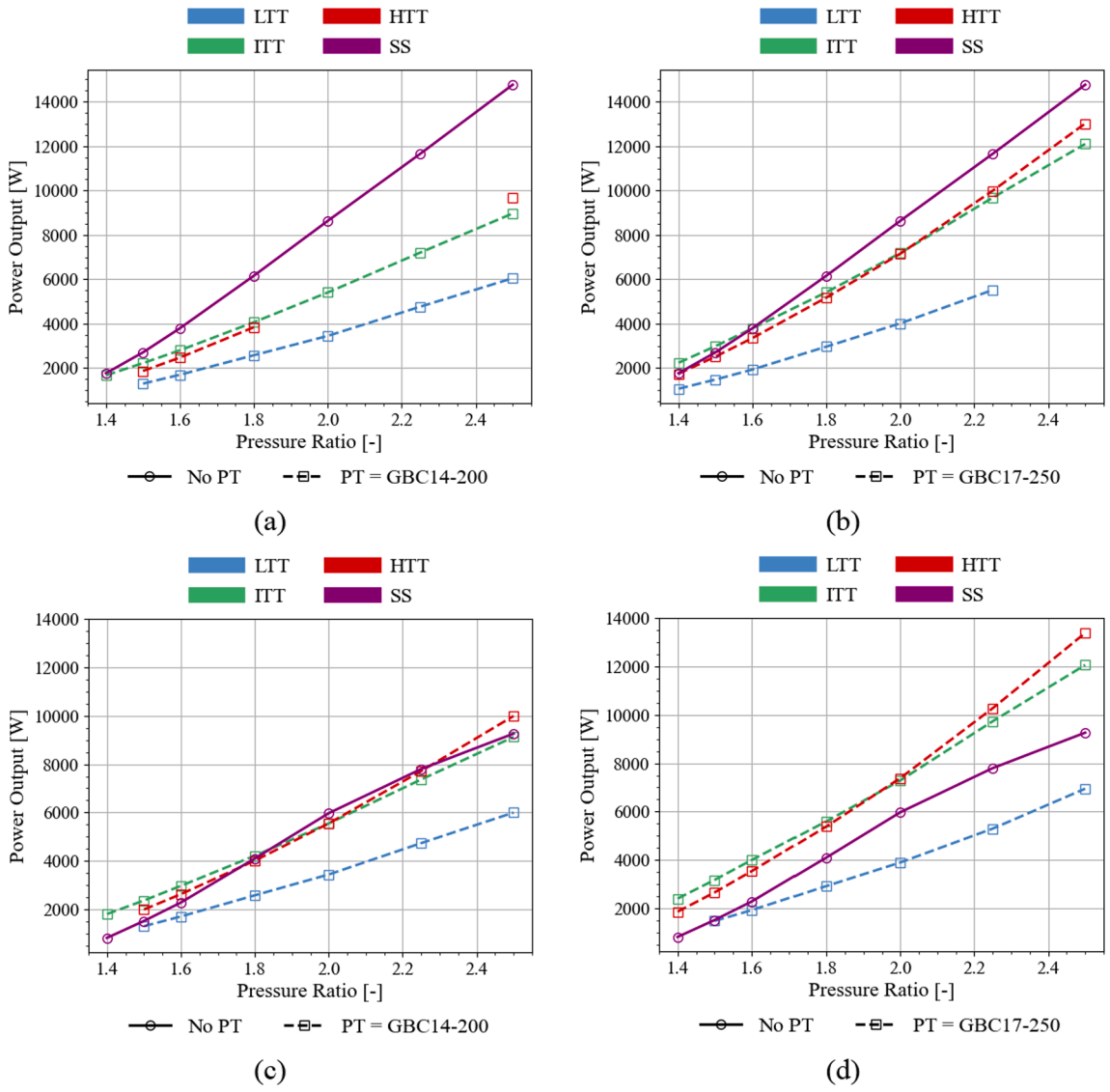

Fig. B3. Power output as a function of pressure ratio in a recuperated cycle for (a) the G25-550 (AR = 0.92) as the GT and GBC14-200 as the PT, (b) the G25-550 (AR = 0.92) as the GT and GBC17-250 as the PT, (c) the GTX4088R (AR = 1.19) as the GT and GBC14-200 as the PT, and (d) the GTX4088R (AR = 1.19) as the GT and GBC17-250 as the PT.

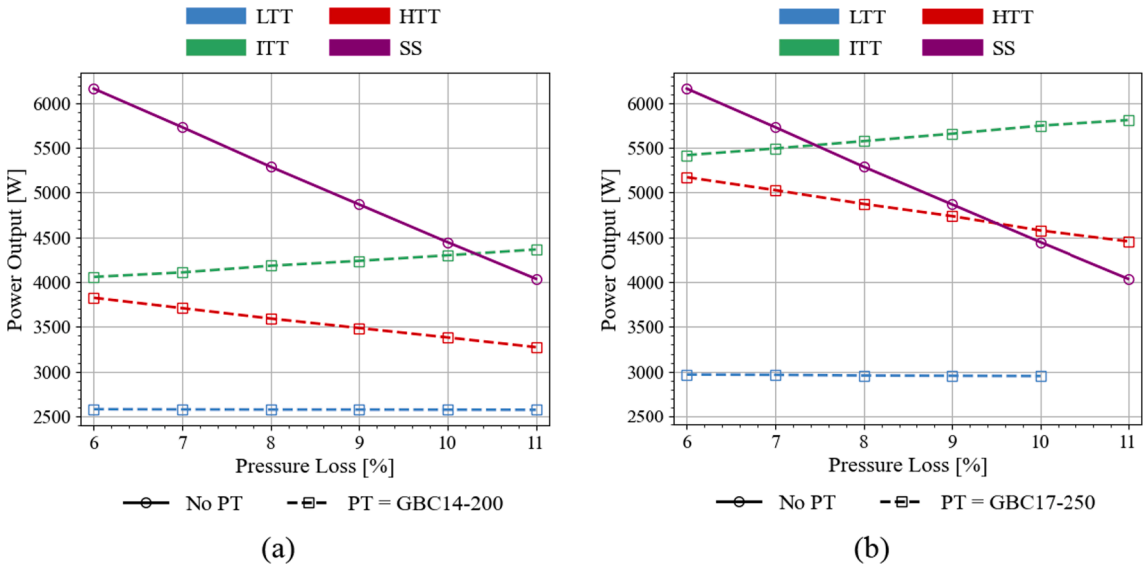

Fig. B4. Power output as a function of pressure loss for the G25-550 (AR = 0.92) as the GT in a recuperated cycle at a compressor pressure ratio of 1.8 with (a) the GBC14-200 as the PT and (b) the GBC17-250 as the PT.

B.3. Simple solar cycle results.

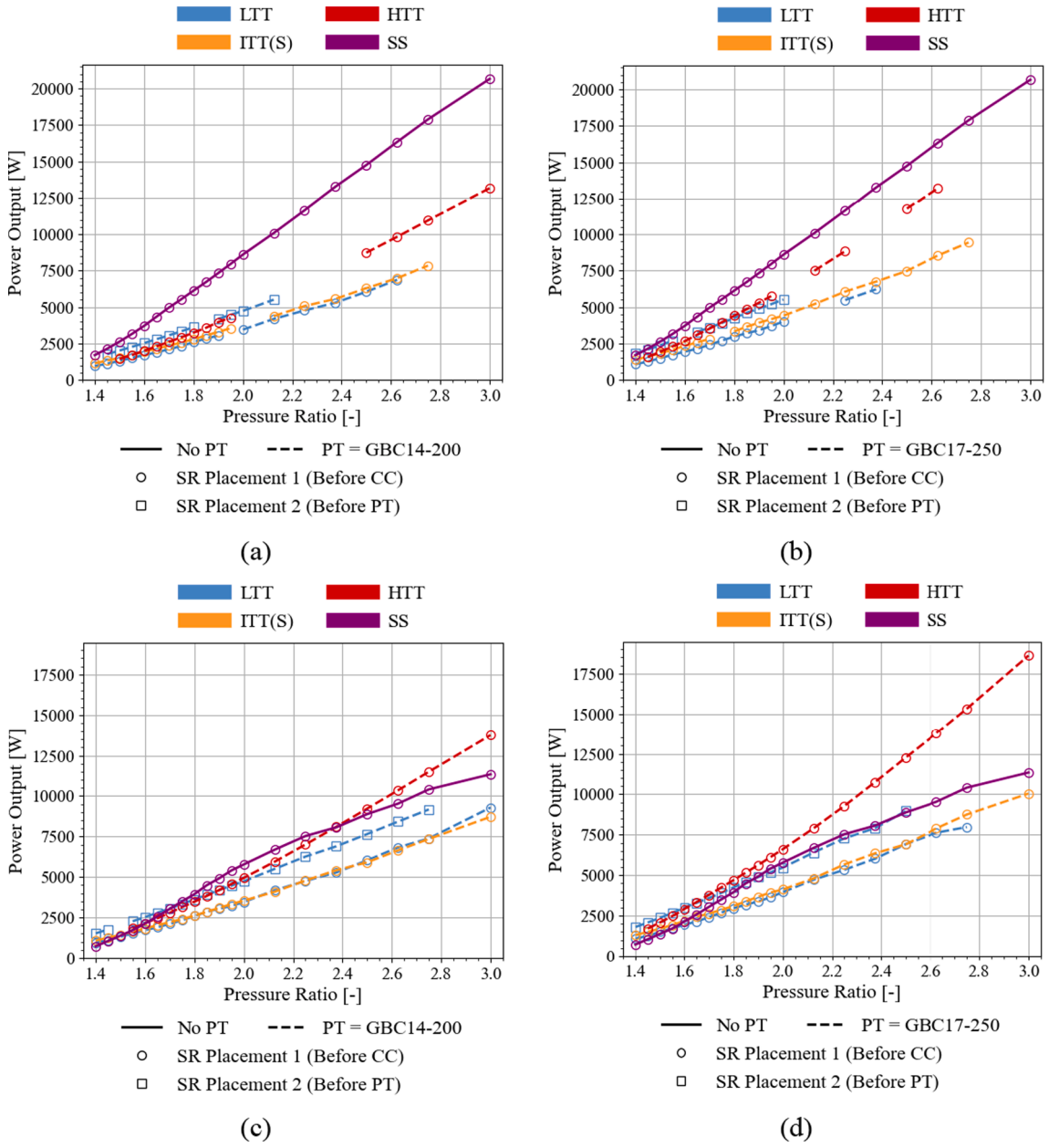

Fig. B5. Power output as a function of pressure ratio in a simple solar cycle for (a) the G25-550 (AR = 0.92) as the GT and GBC14-200 as the PT, (b) the G25-550 (AR = 0.92) as the GT and GBC17-250 as the PT, (c) the GTX4088R (AR = 1.19) as the GT and GBC14-200 as the PT, and (d) the GTX4088R (AR = 1.19) as the GT and GBC17-250 as the PT (adapted from Cockcroft & Le Roux [19]).

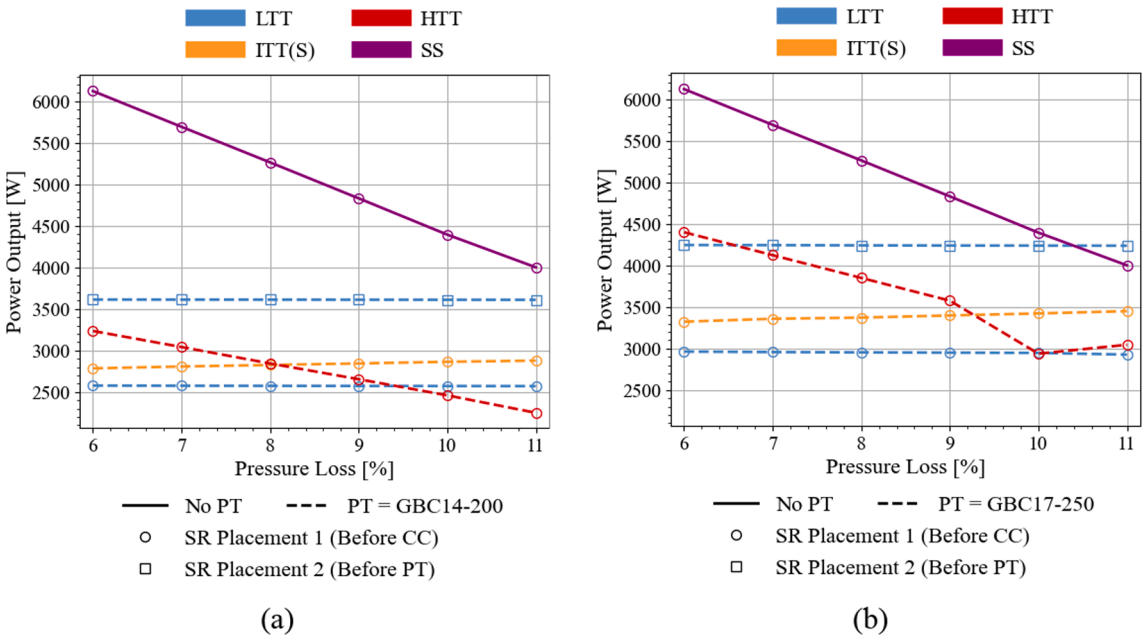

Fig. B6. Power output as a function of pressure loss for the G25-550 (AR = 0.92) as the GT in a simple solar cycle at a compressor pressure ratio of 1.8 with (a) the GBC14-200 as the PT and (b) the GBC17-250 as the PT.

B.4. Recuperated solar cycle results.

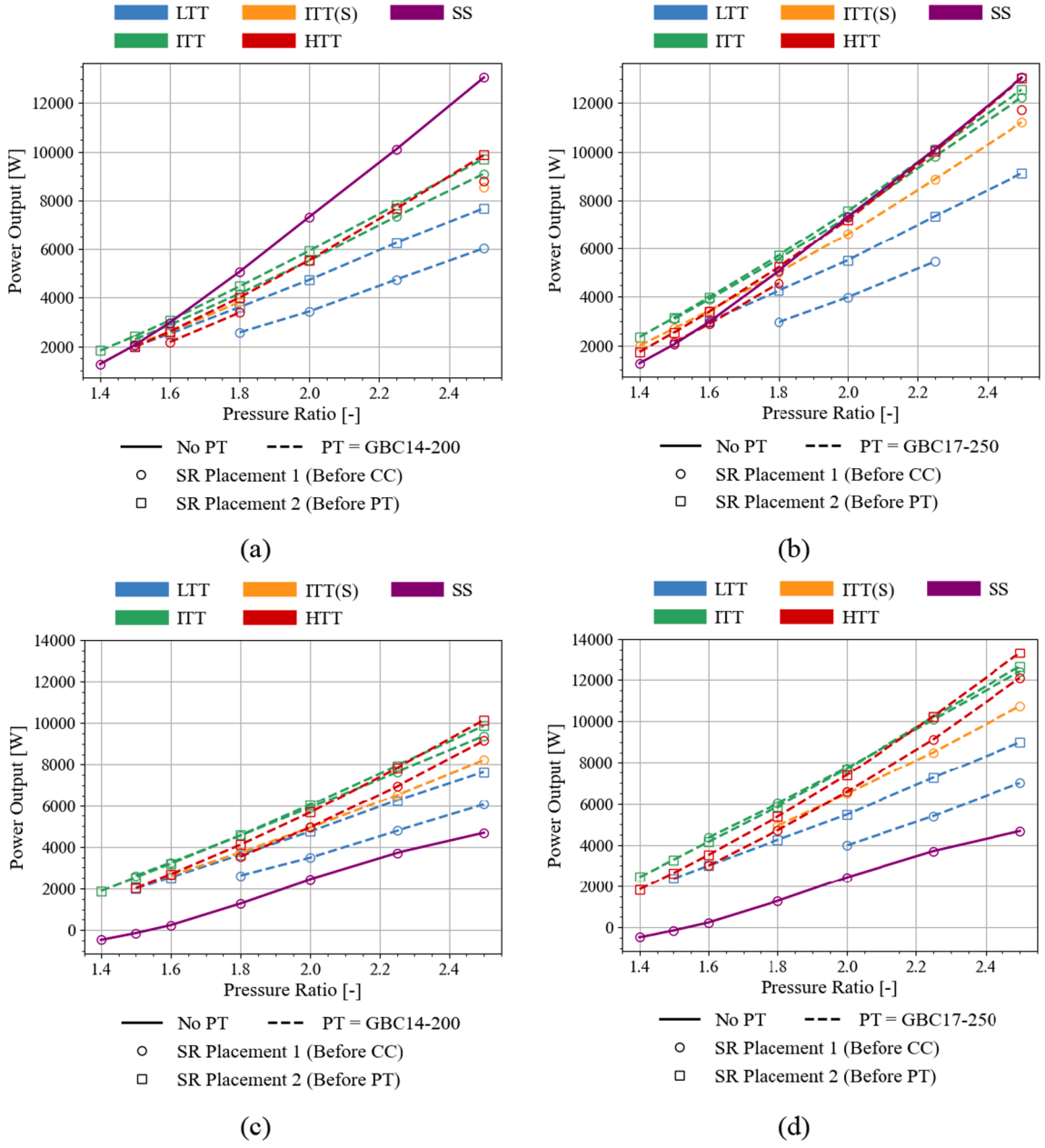

Fig. B7. Power output as a function of pressure ratio in a recuperated solar cycle for (a) the G25-550 (AR = 0.92) as the GT and GBC14-200 as the PT, (b) the G25-550 (AR = 0.92) as the GT and GBC17-250 as the PT, (c) the GTX4088R (AR = 1.19) as the GT and GBC14-200 as the PT, and (d) the GTX4088R (AR = 1.19) as the GT and GBC17-250 as the PT (adapted from Cockcroft & Le Roux [19]).

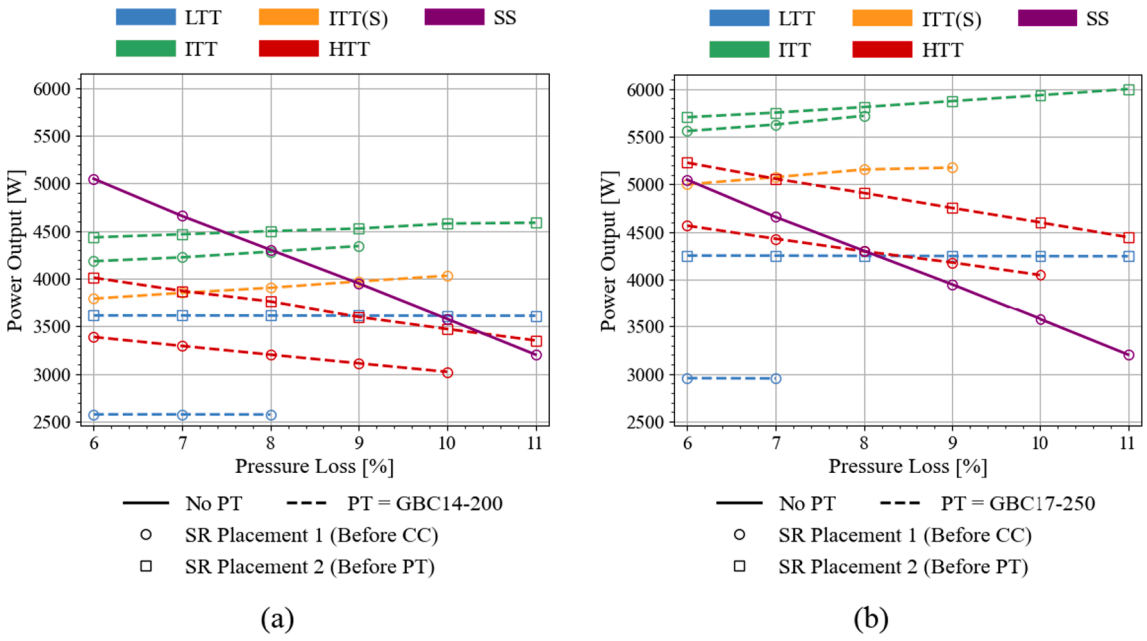

Fig. B8. Power output as a function of pressure loss for the G25-550 (AR = 0.92) as the GT in a recuperated solar cycle at a compressor pressure ratio of 1.8 with (a) the GBC14-200 as the PT and (b) the GBC17-250 as the PT.

Appendix C. Recuperator effectiveness results for the various recuperated and recuperated solar cycles

The recuperator effectiveness results of the various cycles are shown in the sub-sections to follow. These results are important to mention as a higher recuperator effectiveness enables better heat transfer in the recuperator and allows for a greater reduction in the required fuel input.

C.1. Recuperated cycle

When comparing the recuperator effectiveness results in Fig. C1 to the thermal efficiency results in Fig. 11, it is apparent that a higher recuperator effectiveness results in higher thermal efficiencies. It is for this reason that in most instances, the single-shaft recuperator effectiveness is the highest, as these results produce the best thermal efficiency in Fig. 11. The same observation is made for a comparison between Fig. C2 and Fig. 13 when considering increased pressure loss percentages. The higher recuperator effectiveness values directly result from the selected recuperator geometries in Appendix A and the higher hot-side recuperator mass flow rates in the respective cycles. These parameters influence the inlet temperature to the gasifier turbine, thus allowing for greater gasifier turbine outlet temperatures. This creates a greater difference in the cold- and hot-side inlet temperatures of the recuperator, which allows for higher recuperator effectiveness values.

The recuperator effectiveness increases with an increase in pressure loss. This is because a direct result of an increase in pressure loss is higher gasifier turbine inlet temperatures for the parallel-flow cycles, as shown in Fig. 14, which results in increased gasifier turbine exhaust temperatures due to lower gasifier turbine pressure ratios. These higher gasifier turbine exhaust temperatures entail that a higher temperature is entering the hot-side of the recuperator, which increase the temperature difference between the hot-side and the cold-side inlets of the recuperator. This increased temperature difference results in an increase in recuperator effectiveness with an increase in combustion pressure loss, as shown in Fig. C2.

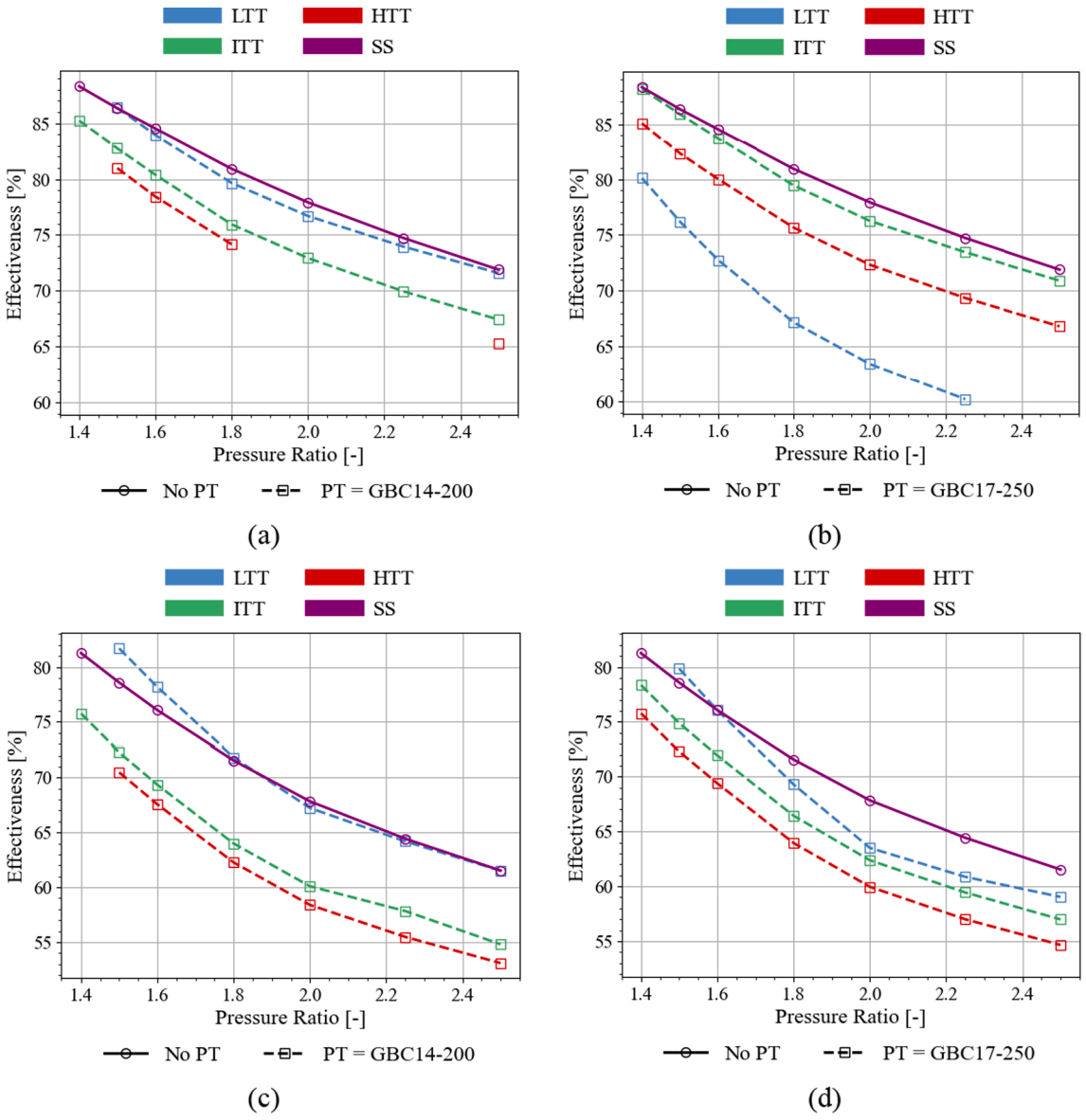

Fig. C1. Recuperator effectiveness as a function of pressure ratio in a recuperated cycle for (a) the G25-550 (AR = 0.92) as the GT and GBC14-200 as the PT, (b) the G25-550 (AR = 0.92) as the GT and GBC17-250 as the PT, (c) the GTX4088R (AR = 1.19) as the GT and GBC14-200 as the PT, and (d) the GTX4088R (AR = 1.19) as the GT and GBC17-250 as the PT.

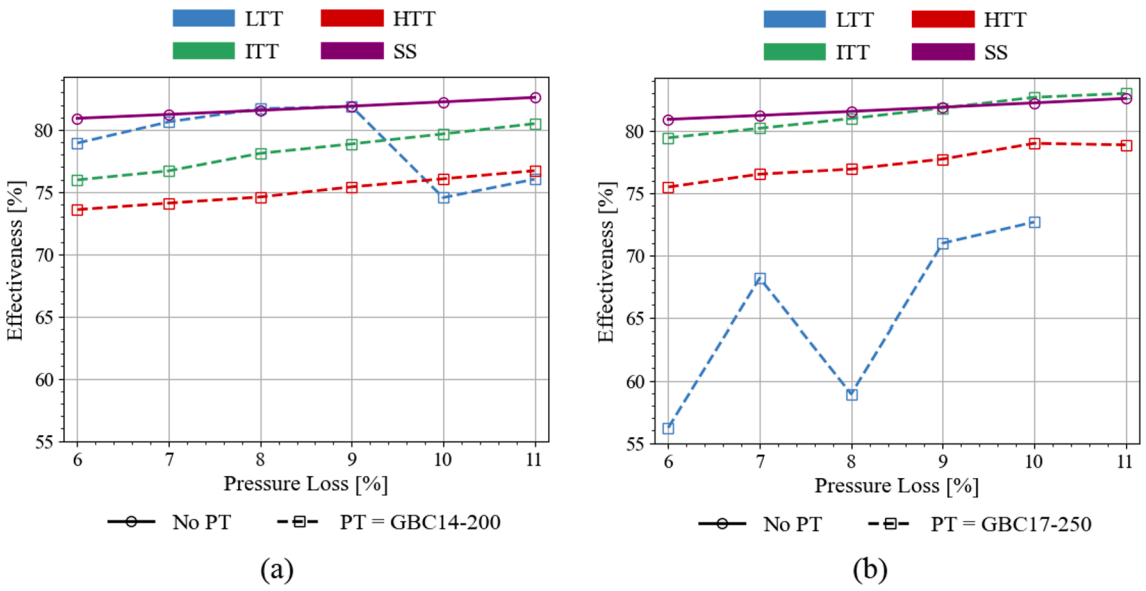

Fig. C2. Recuperator effectiveness as a function of pressure loss for the G25-550 (AR = 0.92) as the GT in a recuperated cycle at a compressor pressure ratio of 1.8 with (a) the GBC14-200 as the PT and (b) the GBC17-250 as the PT.

C.2. Recuperated solar cycle

The recuperator effectiveness values of the recuperated solar cycles, shown in Figs. C3 and C4, allow a similar trend to that of the recuperated cycles, except for regarding the relationship between the recuperator effectiveness and the thermal efficiency values of the single-shaft cycles with the G25-550 (AR = 0.92) main shaft turbocharger. This difference is as a result of a poorer performing recuperator geometry, as shown in Appendix A. This poorer performing single-shaft recuperator geometry allows for lower recuperator effectiveness values. However, this single-shaft cycle still has comparatively higher power output results, as shown in Appendix B.4, thus resulting in higher thermal efficiency values.

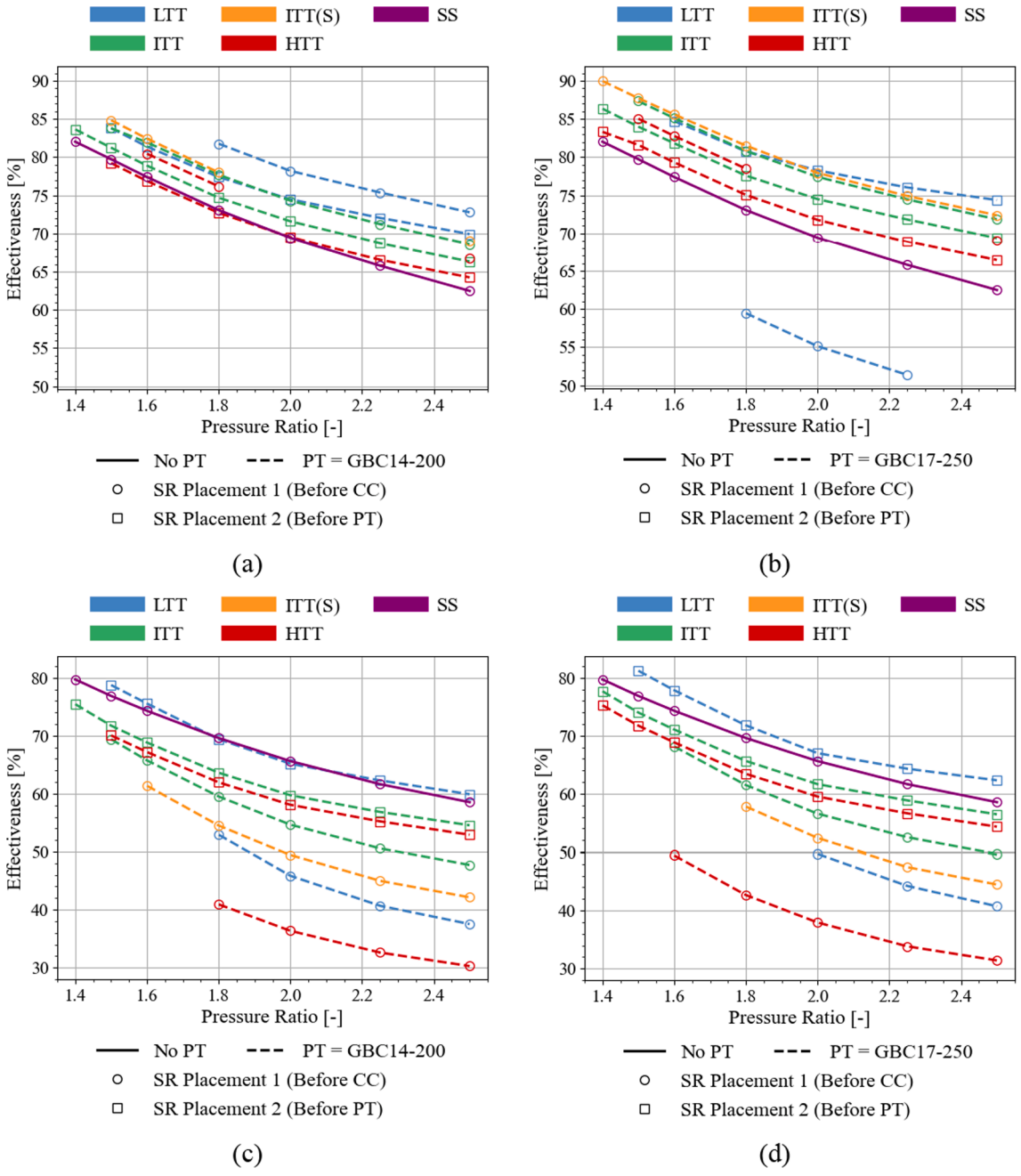

Fig. C3. Recuperator effectiveness as a function of pressure ratio in a recuperated solar cycle for (a) the G25-550 (AR = 0.92) as the GT and GBC14-200 as the PT, (b) the G25-550 (AR = 0.92) as the GT and GBC17-250 as the PT, (c) the GTX4088R (AR = 1.19) as the GT and GBC14-200 as the PT, and (d) the GTX4088R (AR = 1.19) as the GT and GBC17-250 as the PT.

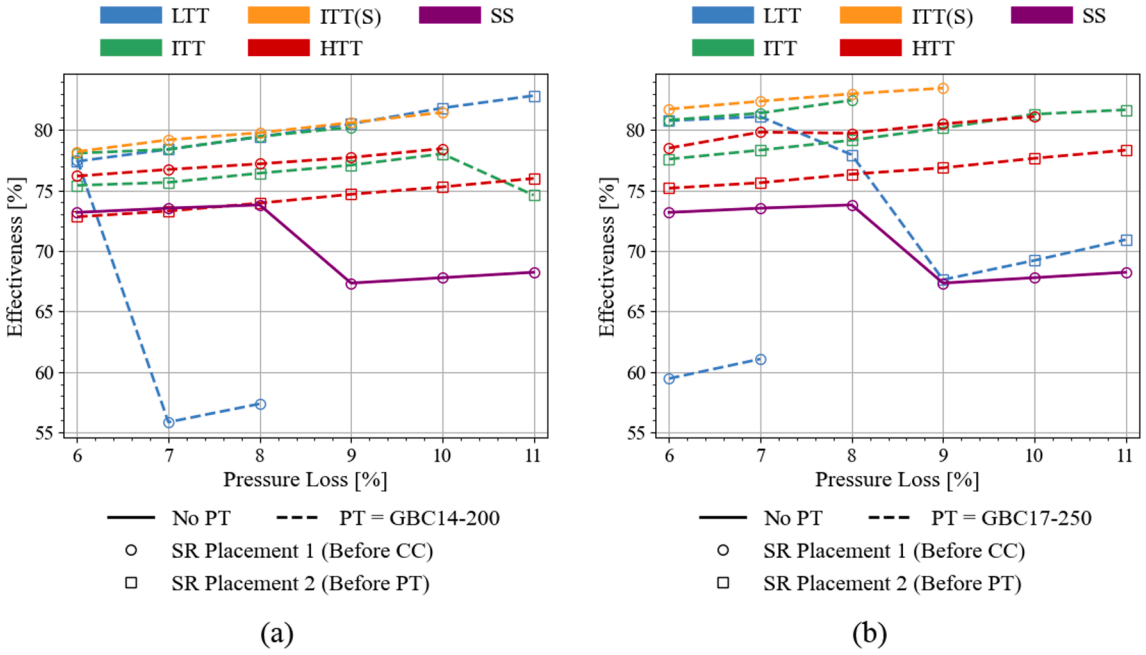

Fig. C4. Recuperator effectiveness as a function of pressure loss for the G25-550 (AR = 0.92) as the GT in a recuperated solar cycle at a compressor pressure ratio of 1.8 with (a) the GBC14-200 as the PT and (b) the GBC17-250 as the PT.

Appendix D. Solar receiver efficiency results for the various recuperated and recuperated solar cycles

The solar receiver efficiency indicates how efficiently each cycle's solar receiver utilises the incoming reflected solar rays and converts the rays into heat for use in the cycle, under a consideration of the mass flow rate of the fluid flowing through the solar receiver. It can be observed from Le Roux et al. [32] that a higher mass flow rate through the solar receiver results in higher receiver efficiencies and that a higher inlet temperature to the solar receiver results in lower solar receiver efficiencies. Thus, a parallel-flow split-off point position and the placement of the solar receiver greatly influences the efficiency of the solar receiver. For split-off points prior to the solar receiver, when the 'SR-CC' receiver placement is used, a lower mass flow rate flows through the solar receiver due to flow split occurring prior to the solar receiver inlet. For the 'SR-PT' placement, there is also an expected lower mass flow rate through the solar receiver due to the parallel-flow cycles operating with a smaller power turbine in comparison to the gasifier turbocharger. Additionally, a split-off point that occurs further along the main flow path, in a 'SR-PT' configuration, will have a higher solar receiver inlet temperature and a subsequent lower solar receiver efficiency.

D.1. Simple solar cycle

The analysis of the influence that the solar receiver efficiency has on the results of the various cycles deviates from that of the influence of the recuperator effectiveness (Appendix C) on the cycles, as a result of the solar receiver placement influencing the results as well. This is as a result of turbines generally performing better with higher turbine inlet temperatures, which increases the power output of the 'SR-PT' placement. Thus, even though the simple solar LTT (SR-PT) cycle has the lowest solar receiver efficiencies in each sub-plot in Figs. D1 and D2, the higher power turbine power output initiated by a higher inlet temperature, as in Appendix B.3, results in better thermal efficiencies for these cycles. It is for the same reason that even though the single-shaft cycles do not have the highest solar receiver efficiencies, these cycles are still able to outperform the higher solar receiver efficiency parallel-flow cycles, even though the single-shaft solar receiver efficiencies may be lower. The power output of the single-shaft cycle with the G25-550 (AR = 0.92) main shaft turbocharger is greater than that of the parallel-flow cycles throughout most of the results in Appendix B.3. However, these single-shaft power output values are lower when the GTX4088R (AR = 1.19) is used as the main shaft turbocharger. This is what causes the higher thermal efficiencies for the G25-550 (AR = 0.92) main shaft turbocharger and the lower thermal efficiencies for the GTX4088R (AR = 1.19) main shaft turbocharger.

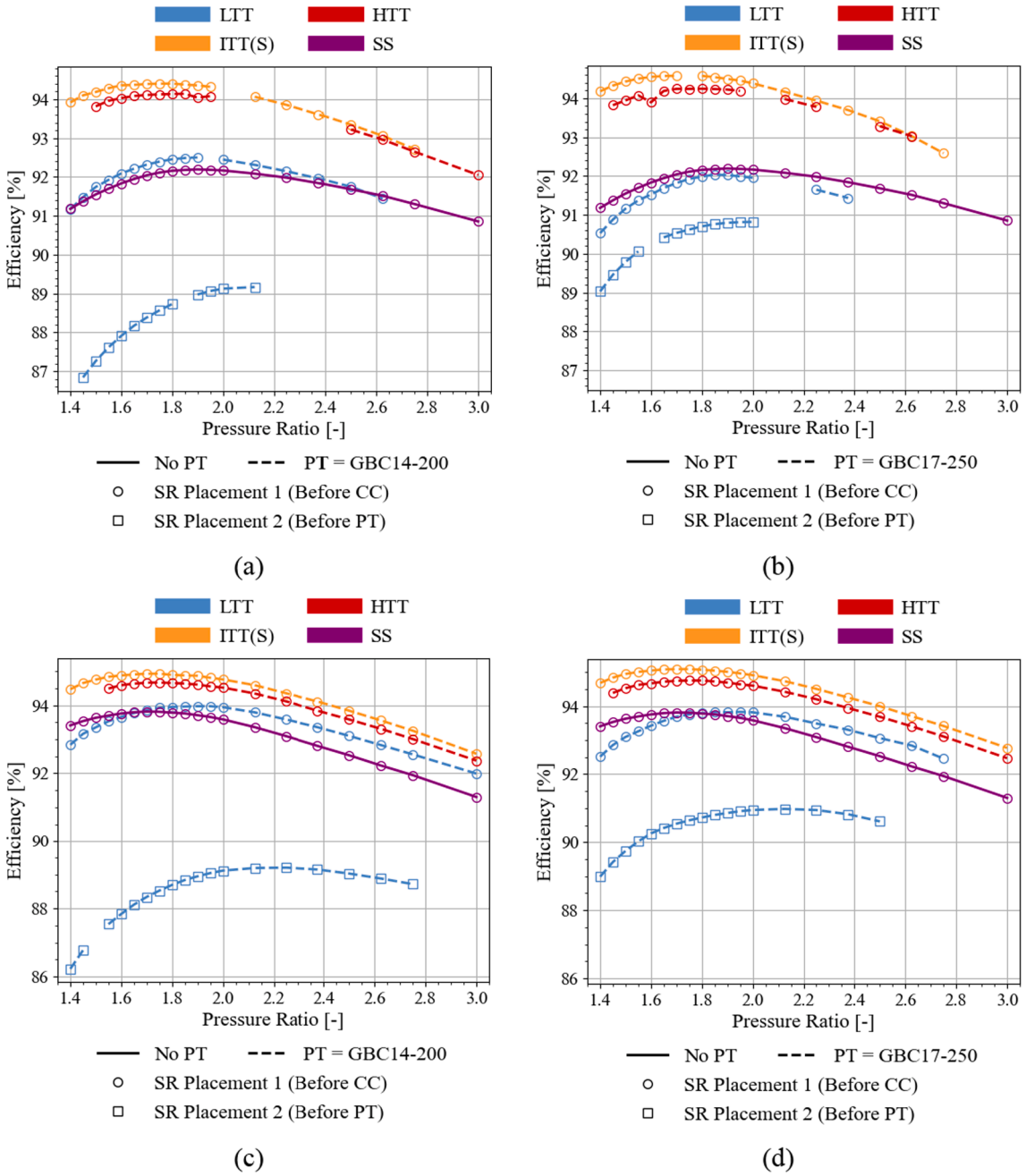

Fig. D1. Solar receiver efficiency as a function of pressure ratio in a simple solar cycle for (a) the G25-550 (AR = 0.92) as the GT and GBC14-200 as the PT, (b) the G25-550 (AR = 0.92) as the GT and GBC17-250 as the PT, (c) the GTX4088R (AR = 1.19) as the GT and GBC14-200 as the PT, and (d) the GTX4088R (AR = 1.19) as the GT and GBC17-250 as the PT (adapted from Cockcroft & Le Roux [19]).

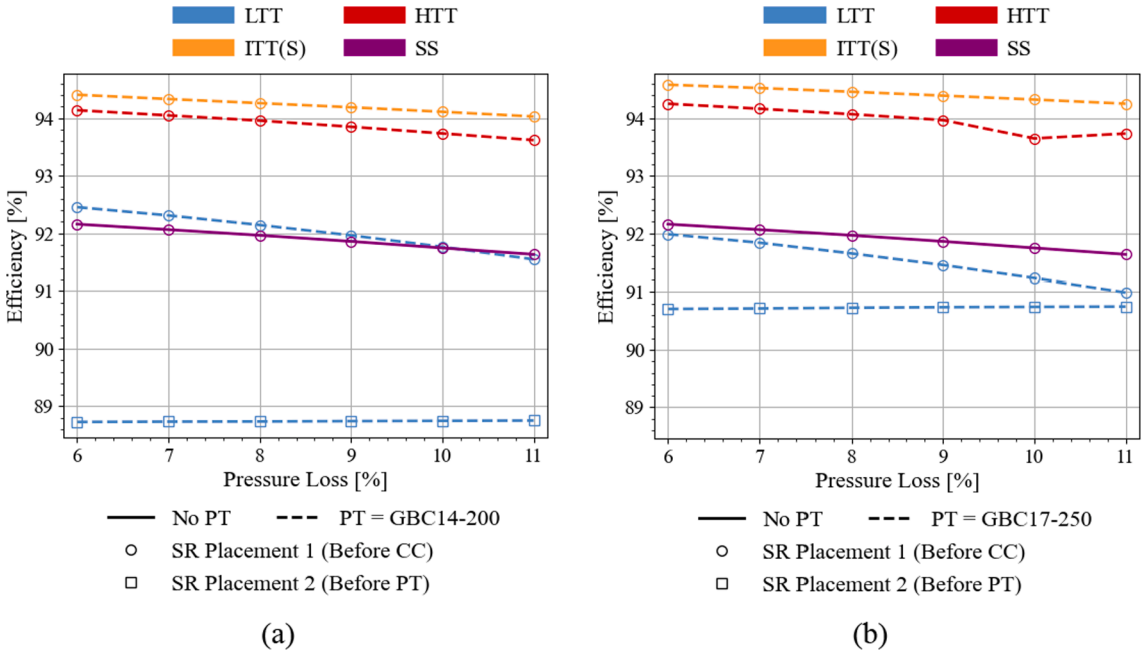

Fig. D2. Solar receiver efficiency as a function of pressure loss for the G25-550 (AR = 0.92) as the GT in a simple solar cycle at a compressor pressure ratio of 1.8 with (a) the GBC14-200 as the PT and (b) the GBC17-250 as the PT.

D.2. Recuperated solar cycle

As in the simple solar cycles, the mass flow rates and solar receiver inlet temperatures influence the efficiency of the solar receiver in a recuperated solar cycle. The recuperated cold-side is placed before the solar receiver in 'SR-CC' and in single-shaft configurations, thus greatly reducing the efficiencies of the solar receivers in these configurations. This is why the LTT (SR-PT) cycles allow for the highest solar receiver efficiencies observed in Figs. D3 and D4. This, along with the observed high recuperator effectiveness values (Appendix C.2.) for these LTT (SR-PT) cycles, allows for the comparatively better thermal efficiencies values in the LTT (SR-PT) configuration.

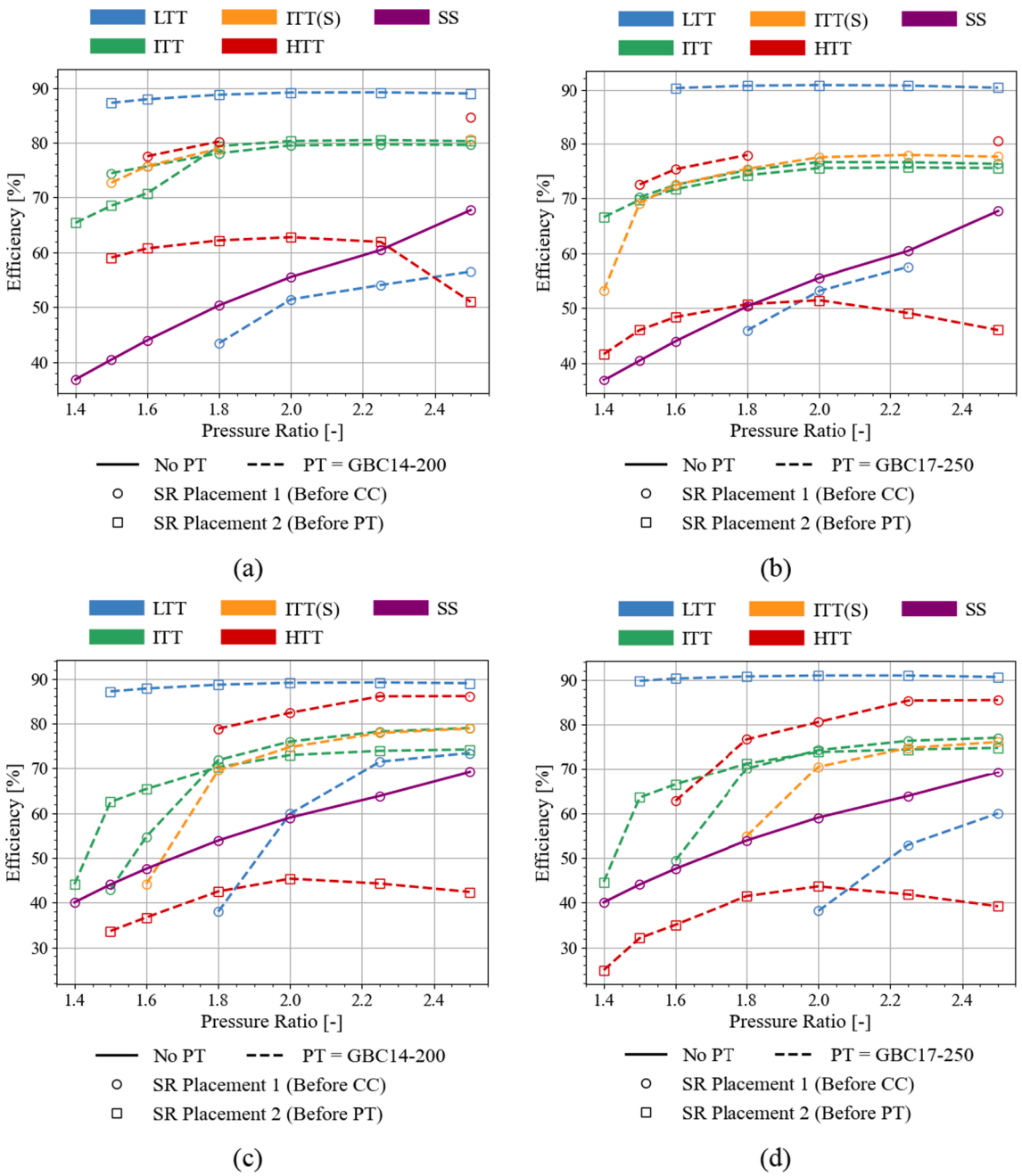

Fig. D3. Solar receiver efficiency as a function of pressure ratio in a recuperated solar cycle for (a) the G25-550 (AR = 0.92) as the GT and GBC14-200 as the PT, (b) the G25-550 (AR = 0.92) as the GT and GBC17-250 as the PT, (c) the GTX4088R (AR = 1.19) as the GT and GBC14-200 as the PT, and (d) the GTX4088R (AR = 1.19) as the GT and GBC17-250 as the PT (adapted from Cockcroft & Le Roux [19]).

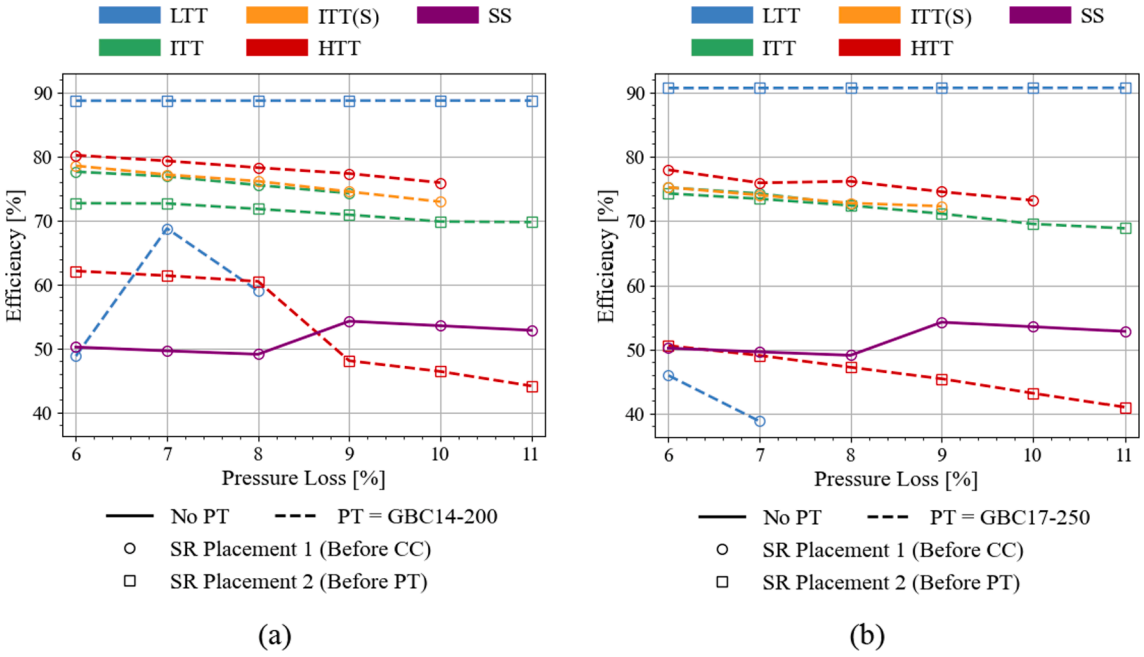

Fig. D4. Solar receiver efficiency as a function of pressure loss for the G25-550 (AR = 0.92) as the GT in a recuperated solar cycle at a compressor pressure ratio of 1.8 with (a) the GBC14-200 as the PT and (b) the GBC17-250 as the PT.

Data availability

Data will be made available on request.

References

[1] Hou H, Lu W, Liu B, Hassanein Z, Mahmood H, Khalid S. Exploring the Role of Fossil Fuels and Renewable Energy in Determining Environmental Sustainability: Evidence from OECD Countries. *Sustainability* 2023;15(3):2048.

[2] J. Lou, J. Wang, J. Xia, Y. Du, P. Zhao and G. Zhang, "Thermodynamic analysis of open-air Brayton cycle to predict radial turbine aerodynamic performance," *Applied Thermal Engineering,* vol. 219, no. A, 2023.

[3] Toker SC, Soyturk G, Kizilkan O. Development of a sustainable multi-generation system with re-compression sCO2 Brayton cycle for hydrogen generation. *Int J Hydrogen Energy* 2022;47(45):19397–410.

[4] U.S. Department of Energy, "Chapter 4: Advancing Clean Electric Power Technologies," 1 June 2016. [Online]. Available: https://www.energy.gov/sites/prod/files/2016/06/f32/QTR2015-4R-Supercritical-Carbon-Dioxide-Brayton%20Cycle.pdf. [Accessed 6 August 2024].

[5] Mozzhegorova Y, Ilinykh G, Korotaev V. Life Cycle Assessment of a Gas Turbine Installation. *Energies* 2024;17(2):1–24.

[6] Meana-Fernández A, González-Caballín JM, Martínez-Pérez R, Rubio-Serrano FJ, Gutiérrez-Trashorras AJ. Power Plant Cycles: Evolution towards More Sustainable and Environmentally Friendly Technologies. *Energies* 2022;15(23):8982.

[7] T. Akba, D. K. Baker and M. Pınar Mengüç a, "Off-design performance of micro-scale solar Brayton cycle," *Energy Conversion and Management,* vol. 289, 2023.

[8] Jouhara H, Khordehgah N, Almahmoud S, Delpech B, Chauhan A, Tassau SA. Waste heat recovery technologies and applications. *Therm Sci Eng Prog* 2018;6:268–89.

[9] Sheintuch M, Nekhamkina O, Tartakovsky L. Heat Recuperation from Internal Combustion Engines by Fuel Reforming: Kinetics-Based Analysis. *ACS Eng Au* 2023;3(3):210–23.

[10] Hwang G, Jeong S. Pressure loss effect on recuperative heat exchanger and its thermal performance. *Cryogenics* 2010;50(1):13–7.

[11] Visser WPJ, Shakariyants SA, Oostveen M. Development of a 3 kW Microturbine for CHP Applications. *J Eng Gas Turbines Power* 2011;133(4):1–8.

[12] W. G. Le Roux, "Feasibility study of a hybrid small-scale dish-mounted solar thermal Brayton cycle with cogeneration," in *International Heat Transfer Conference*, 2018, 10-15 August, pp. 7929–7936. https://doi.org/10.1615/IHTC16.nee.024185.

[13] Le Roux WG, Sciacovelli A. Recuperated solar-dish Brayton cycle using turbocharger and short-term thermal storage. *Sol Energy* 2019;194(2019):569–80.

[14] Butt MU. "Converting an automobile turbocharger into a micro gas turbine," in *The 3rd International Conference on Power, Energy and Mechanical Engineering (ICPEME 2019)*. Prague: Czech Republic; 2019.

[15] De Beer JH, Le Roux WG, Sciacovelli A, Meyer JP. Effect of a novel cooling window on a recuperated solar-dish Brayton cycle. *Renew Energy* 2023;208:465–80.

[16] Van der Merwe AH, Le Roux WG, Humphries ED. Parallel turbochargers for small-scale power generation. *Appl Therm Eng* 2023;235:1–23.

[17] Kim J-S, Kim D-Y, Kim Y-T. Experiment on radial inflow turbines and performance prediction using deep neural network for the organic Rankine cycle. *Appl Therm Eng* 2019;149:633–43.

[18] Swanepoel JK, Le Roux WG, Roosendaal C, Madani SH, De Wet G, Nikolaidis T, et al. Initial experimental testing of a hybrid solar-dish Brayton cycle for combined heat and power (ST-CHP). *Appl Therm Eng* 2024;249:1–22.

[19] Cockcroft CC, Le Roux WG. The influence of applying a solar dish to parallel-flow configurations of a Brayton cycle. *Sol Energy* 2025;288.

[20] Herdzik J. Impact of pressure drop in combustion chamber on gas turbine performance. *Journal of Civil Engineering and Transport* 2020;2(3):131–8.

[21] Fatsis A. Design point analysis of two-shaft gas turbine engines topped by four-port wave rotors for power generation systems. *Propul Power Res* 2019;8(3):183–93.

[22] Cockcroft CC, Le Roux WG. The influence of applying turbine inlet air cooling to a small-scale parallel-flow Brayton cycle. *Energ Conver Manage* 2025;325.

[23] Cockcroft CC, Le Roux WG. A comparative analysis between small-scale recuperated parallel-flow Brayton cycles. *Appl Therm Eng* 2025;267.

[24] Le Roux WG, Bello-Ochende T, Meyer JP. "Optimisation of an open rectangular cavity receiver and recuperator used in a small-scale solar thermal Brayton cycle with thermal losses. 10th International Conference on Heat Transfer. Orlando: Fluid Mechanics and Thermodynamics; 2014.

[25] Garrett Motion, "Garrett Performance Turbo," 2023. [Online]. Available: https://www.garrettmotion.com/racing-and-performance/performance-turbos/?term_id=28. [Accessed 11 May 2023].

[26] Automeris, "Extract data from charts," 2024. [Online]. Available: https://automeris.io/. [Accessed 2 August 2024].

[27] Garrett Motion, "GARRETT G42-1200 73MM," 2024. [Online]. Available: https://www.garrettmotion.com/racing-and-performance/performance-catalog/turbo/g-series-g42-1200/. [Accessed 2 August 2024].

[28] W. G. Le Roux and J. P. Meyer, "Modeling the Small-Scale Dish-Mounted Solar Thermal Brayton Cycle," in *AIP Conference Proceedings*, Vol. 1734, No. 1, AIP Publishing, 2016, https://doi.org/10.1063/1.4949144.

[29] Rankokwane B, Makhurutha SE, Makhurutha T, Motlasuping T. LIQUEFIED PETROLEUM GAS MARKET STUDY. Lobatse: Botswana Energy Regulatory Authority; 2021.

[30] Lefebvre H, Ballal DR. Gas Turbine Combustion: Alternative Fuels and Emissions. 3rd ed. Boca Raton: Taylor and Francis Group, LLC; 2010.

[31] Nellis GF, Pfotenhauer JM. Effectiveness-NTU Relationship for a Counterflow Heat Exchanger Subjected to an External Heat Transfer. *J Heat Transfer* 2005;127:1071–3.

[32] Le Roux WG, Bello-Ochende T, Meyer JP. The efficiency of an open-cavity tubular solar receiver for a small-scale solar thermal Brayton cycle. *Energ Conver Manage* 2014;84:457–70.

[33] The National Renewable Energy Laboratory, "SolTrace," [Online]. Available: https://www.nrel.gov/csp/soltrace.html. [Accessed 20 August 2024].